

TR-91-06

2

AD-A236 353



Final Report

Optical Fibre Based Frequency Shifters Project

Contract Number: F49620-88-C-0123

This report has been reviewed and is releasable to the National Technical Information Service (NTIS).
At NTIS it will be releasable to the general public, including foreign nations.

This technical report has been reviewed and is approved for publication.



PARRIS C. NEAL, Lt Col, USAF
Chief, Applied Electronics



FRED T. GILLIAM, Lt Col, USAF
Chief Scientist



41003505 711
NTIS
DTIC
JAN 1971
A-1

REPORT DOCUMENTATION PAGE

Form Approved
OMB No. 0704-0188

Public reporting burden for this collection of information is estimated to average 1 hour per response, including the time for reviewing instructions, searching existing data sources, gathering and maintaining the data needed, and completing and reviewing the collection of information. Send comments regarding this burden estimate or any other aspect of this collection of information, including suggestions for reducing this burden, to Washington Headquarters Services, Directorate for Information Operations and Reports, 1215 Jefferson Davis Highway, Suite 1204, Arlington, VA 22202-4302 and to the Office of Management and Budget, Paperwork Reduction Project (0704-0188), Washington, DC 20503.

1. AGENCY USE ONLY (Leave blank)	2. REPORT DATE 28 Jan 91	3. REPORT TYPE AND DATES COVERED Final, 1 Jan 89 - 31 Dec 90
---	------------------------------------	--

4. TITLE AND SUBTITLE Optical Fibre Based Frequency Shifters Project	5. FUNDING NUMBERS FL 49620-88 - C-0123
--	--

6. AUTHOR(S) Mr. M. Berwick and Professor D.A. Jackson	
--	--

7. PERFORMING ORGANIZATION NAME(S) AND ADDRESS(ES) University of Kent at Canterbury, Department of Physics, CANTERBURY, Kent. CT2 7NR.	8. PERFORMING ORGANIZATION REPORT NUMBER
--	---

9. SPONSORING/MONITORING AGENCY NAME(S) AND ADDRESS(ES) European Office of Aerospace Research and Development PO Box 14, FPO New York 09510-0200	10. SPONSORING/MONITORING AGENCY REPORT NUMBER TR-91-06
--	---

11. SUPPLEMENTARY NOTES

12a. DISTRIBUTION/AVAILABILITY STATEMENT Approved for public release Distribution unlimited.	12b. DISTRIBUTION CODE
---	-------------------------------

13. ABSTRACT (Maximum 200 words) This report summarises the research programme to develop acousto-optic frequency shifters based on highly linearly birefringent optical fibre. The theory of operation, fabrication and performance of devices utilising either flexural or torsional acoustic waves is presented.

Research directed towards a flexural acoustic wave fibre frequency shifter lead us to the conclusion that this technique is not suitable for the production of a high efficiency device. The research into torsional acoustic wave fibre frequency shifters has enabled the fabrication of devices with two different designs of torsional acoustic wave generator: (i) a side-fibre design and (ii) an in-line acoustic horn design. The fibre frequency shifters constructed from these generators produce a shift in the optical frequency of about 3MHz.

A fibre frequency shifter constructed using the former design had a maximum optical power coupling efficiency of 6%; with an electrical power of 780mW applied to the transducer. Unfortunately, this design is rather fragile, hence a large proportion of research effort has been devoted to the design and fabrication of the more rugged in-line acoustic horns. The maximum optical power coupling efficiency achieved to date with this design of fibre frequency shifter is about 2.5%.

14. SUBJECT TERMS An acousto-optic frequency shifter, highly birefringent optical fibre, torsional acoustic wave, side-fibre design, in-line acoust	15. NUMBER OF PAGES
---	----------------------------

	16. PRICE CODE c.horn.
--	----------------------------------

17. SECURITY CLASSIFICATION OF REPORT UNCLASSIFIED	18. SECURITY CLASSIFICATION OF THIS PAGE UNCLASSIFIED	19. SECURITY CLASSIFICATION OF ABSTRACT UNCLASSIFIED	20. LIMITATION OF ABSTRACT
--	---	--	-----------------------------------

4.3.5 Possible improvements.	34
4.4 Torsional hibi frequency shifter II: 'In-line' configuration.	41
4.4.1 Introduction.	41
4.4.2 Fabrication of piezoelectric drive.	43
4.4.2.1 Bow-tie	43
4.4.2.2 Side shear plates.	44
4.4.2.3 Base mounted pzt shear plates.	44
4.4.3 Fabrication of acoustic horns.	46
4.4.3.1 Introduction.	46
4.4.3.2 Pyrex capillary drawn onto tungsten wire.	48
4.4.3.3 Ground tapered Pyrex capillary.	48
4.4.3.4 Drilling.	50
4.4.3.5 Drawn Pyrex capillary horn (type F).	51
4.4.4 Measurement of torsional vibration.	52
4.4.4.1 Introduction.	52
4.4.4.2 Evaluation of type A torsional transducer.	52
4.4.4.3 Measurement of vibration along the acoustic horn.	53
4.4.5 Results of torsional measurements.	54
4.4.5.1 Type B transducer with solid silica horn.	54
4.4.5.2 Type C transducer with solid silica horn.	54
4.4.5.3 Type C transducer with ground tapered Pyrex capillary horn.	55
4.4.5.4 Type C transducer with type F drawn Pyrex capillary horn.	60

4.4.6 In-line torsional fibre frequency shifter.	61
4.4.6.1 Fabrication of in-line shifter.	61
4.4.6.2 Results and discussion.	61
5 Alternative frequency shifter configurations.	66
5.1 Surface waves on a piezoelectric cylinder.	66
5.2 Stimulated Brillouin scattering.	68
5.3 Two frequency lasers.	68
5.4 Two spatial mode filter.	69
Acknowledgement.	69
References.	70

Summary

This report summarises the results of the research programme carried out by the Applied Optics Group at the University of Kent at Canterbury, U.K., on the development of optical fibre based frequency shifters. This work was funded by the United States Air Force Office of Scientific Research, under Contract F49620-88-C-0123, during the period 1/1/89 to 31/12/90. The principal investigator for this project was Prof. D.A. Jackson and the research associate was Mr M. Berwick. The report includes work completed during the final period of the project, 30/10/90 to 31/12/90, which has not been previously reported.

A fibre optic frequency shifter can be used to replace the Bragg cell acousto-optic modulator, currently used to generate low frequency optical carriers, in fibre optic communications and sensor systems. This new form of frequency shifter, being an all fibre device, in which the propagating optical beam is always guided, offers significantly higher optical efficiencies when compared with the Bragg cell.

Most of the effort has been directed to the research and evaluation of two different types of frequency shifter, which may be classified as (i) flexural and (ii) torsional acoustic wave devices. Both classes of device make use of the two orthogonally polarised eigenmodes of a highly linearly birefringent optical fibre. The theory of operation, design, methods of fabrication and evaluation of performance of each device are presented.

The work towards a flexural acoustic wave fibre frequency shifter leads us to the conclusion that this technique is not suitable for the production of a high efficiency device. The work towards a torsional acoustic wave fibre frequency shifter has enabled the fabrication of devices with two different designs of torsional acoustic wave generator: (i) a side-fibre design and (ii) an in-line acoustic horn design. The fibre frequency shifters constructed from these generators produce a shift in the optical frequency of ~3MHz.

A fibre frequency shifter constructed using the former design had a maximum optical power coupling efficiency (the fraction of the input optical power which is shifted in frequency by the device) of 6%; with an

electrical power of 780mW applied to the transducer. Unfortunately, this design is rather fragile, hence a large proportion of the research effort has been devoted to the design and fabrication of the more rugged in-line acoustic horns. The maximum optical power coupling efficiency achieved, to date, with this design of fibre frequency shifter is ~2.5%. The theory presented demonstrates that 100% coupling efficiencies are attainable and the future work, discussed in the report, promises to yield fibre frequency shifters with efficiencies approaching the theoretical maximum.

1 Introduction

The production of a continuous heterodyne carrier at a suitable frequency for signal processing is an essential feature of many optical fibre sensor systems [1]. Consequently, an optical frequency shifter in fibre form (as opposed to a bulk-optic device such as a Bragg cell) would be a highly desirable component and the development of such devices has attracted a large number of workers in recent years, (for example references [2-8] and those contained therein). The main elements of a fibre-optic frequency shifter are firstly, an optical fibre which in its unperturbed state supports two initially orthogonal optical modes and secondly, a means of inducing a perturbation in such a way that, in the perturbed state, optical power can be efficiently exchanged between the modes (see figure 1-1). If the power coupling is achieved with a travelling perturbation then the coupled light will be shifted in frequency with respect to the uncoupled light.

Both linearly birefringent fibre (for example [1,3,6]), and overmoded optical fibre (for example [5]), capable of supporting the two lowest order spatial modes (LP₀₁ and LP₁₁), have been used in work reported so far. The method of inducing the travelling perturbation has been to either induce surface acoustic waves on a planar substrate [2,3,8] or a cylindrical substrate [4] against which the fibre is clamped, or by means of a flexure wave induced on the fibre itself [5,6,7]. In the first class of device the mechanism of mode coupling is that of pressure-induced changes in refractive index, whilst in the second, the refractive index of the fibre is modified by microbending. In both classes the frequency shift arises due to the travelling nature of the perturbation. The class of device in which the acoustical wave is excited on the 'free' fibre is inherently more efficient than the substrate type; this is simply a consequence of the more efficient concentration of acoustic energy into the vicinity of the fibre core.

As an example of typical relative efficiencies of the 'substrate type' and 'free fibre' devices, a substrate device [8] constructed from a slab of PZT 4, onto which interdigital transducers were deposited, had a quoted optical conversion efficiency of ~25%, at a continuous electrical power of 6.5 watt. This device was based upon birefringent fibre of circular cross-section, with an interaction length of approximately 30mm and operated at a frequency of 3MHz (the frequency at which the acoustic wavelength equals the fibre beat length).

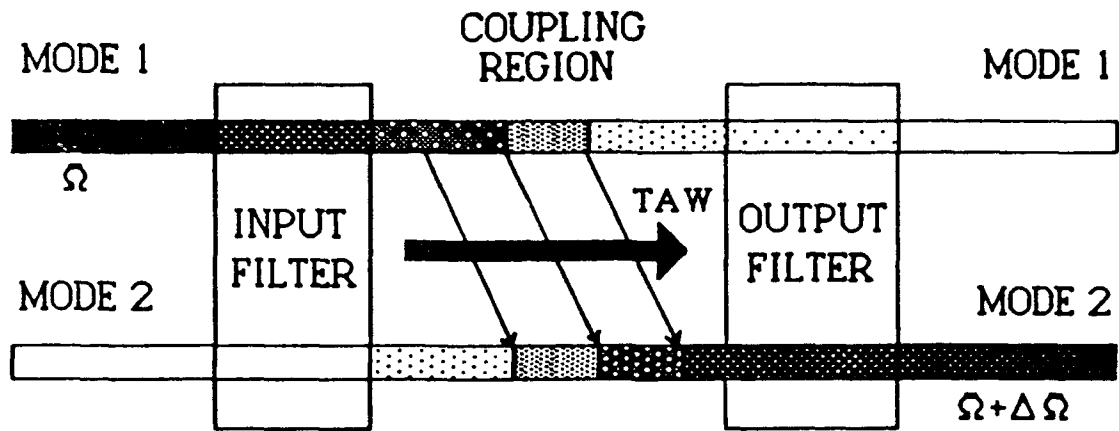


Figure 1-1 : Schematic of an optical fibre frequency shifter.
(TAW = travelling acoustic wave)

In contrast a free fibre device reported in reference [5], produced an optical conversion efficiency of 100% at a continuous input electrical power of 0.25 watt. This device was based upon a two-moded fibre, where the frequency of the perturbing flexure wave was 8 MHz, corresponding to a wavelength in quartz fibre equal to the LP₀₁/LP₁₁ 'beat length'.

Both classes of device, substrate and free fibre, have advantages and disadvantages. The substrate device is potentially more rugged and is tunable [3]. It uses ordinary birefringent fibre, producing a frequency shifted output in the lowest order fibre mode. The free fibre devices employing acoustic flexure waves to effect mode coupling tend to be more efficient, but as the light is coupled into higher order fibre modes, this involves extra optical complexity and requires the use of filters, static mode converters, and, preferably, elliptical core fibres to ensure a stable fundamental mode output.

2 Outline of project

The initial stage of this project constituted a literature review and theoretical study of previous work carried out in the field of optical fibre based frequency shifters. Previous work carried out at the University of Kent [6] was based on the excitation of flexure waves directly onto a highly birefringent fibre, hence this work was the basis of this project. Although other configurations were considered (see section 5), we decided to concentrate our efforts on frequency shifters with highly birefringent fibre, on the basis that it will then be easier to incorporate the device into existing sensor systems employing similar fibre. In order to take advantage of the potential high efficiency, a free fibre construction has been used.

With these constraints, it is necessary to determine which type of acoustic wave propagating on a birefringent fibre is the most efficient at effecting mode conversion. It is shown, for example in reference [9], that the travelling acoustic waves which may be excited on a rod fall broadly into three categories, longitudinal, torsional and flexural. Of these three, the longitudinal modes are of no direct use in the present context as they are independent of the transverse co-ordinates and consequently produce no mode coupling. The flexural mode of lowest order was investigated, however experimental and theoretical analysis, given in sections 3 and 4, has shown that this acoustic mode produces only a small effect and is

inherently incapable of yielding a birefringent fibre frequency shifter of high efficiency. It is the exploration of the third class of excitations, the torsional modes, which has proved the most advantageous. We have derived the coupling coefficient for a fundamental torsional mode in terms of its peak angular displacement, and have demonstrated the use of such a mode to produce a frequency shift in a birefringent fibre, with two different torsional transducer configurations. As will be shown below, the advantages of using torsional, rather than flexural, acoustic waves, to couple the eigenmodes of a highly birefringent fibre, are increased coupling efficiency, higher frequency shifts; corresponding to higher signal processing bandwidths, and the removal of the necessity for eigenaxis alignment.

A non-contact, heterodyne interferometric linear vibrometer was also developed and used as an analytical tool to measure the vibration amplitudes and distributions, throughout the development of the optical fibre frequency shifter systems.

3 Flexural acoustic wave fibre frequency shifters.

3.1 Theory

The theory of operation of optical fibre frequency shifters is covered by the so-called 'coupled mode theory'[10]. The basic approach, common to all fibre frequency shifter configurations, is given in this section. The method may be extended to derive the coupling coefficient corresponding to the specific coupling mechanism utilised. This has been reported for several configurations [6,12]; and chapter VI of reference [11] is devoted to a complete analysis of the use of flexural waves to couple the eigenmodes of highly birefringent fibre. In section 4.2 of this report, the derivation of the coupling efficiency of torsional acoustic waves with highly birefringent fibre, is presented.

If the two modes (polarisation eigenmodes, say) have associated amplitudes $A_1(z)$ and $A_2(z)$ then the coupled mode equations may be written as

$$\frac{dA_1(z)}{dz} = -i \kappa^{(m)} A_2(z) e^{(i \Delta\beta z)} \quad (1)$$

$$\frac{dA_2(z)}{dz} = -i \kappa^{(m)*} A_1(z) e^{(-i \Delta\beta z)} \quad (2)$$

$$\Delta\beta = \beta_1 - \beta_2 - mK \quad (3)$$

where β_1 and β_2 are the propagation constants of the two modes and K is the angular wavenumber of the perturbation, which is propagating co-directionally with the light in the two modes. $\kappa^{(m)}$ is the coupling coefficient for the two modes. Derivation of equations (1 and 2) from the wave equation applied to unperturbed and perturbed expressions for the modal electric fields;

$$\left[\nabla^2 - \mu \epsilon_0(x,y) \frac{\delta^2}{\delta t^2} \right] \mathbf{E} = 0 \quad (4)$$

gives the following definition for the coupling constant

$$\kappa^{(m)} \equiv \frac{\omega}{4} \iint E_1^* \epsilon_m(x,y) E_2 dA \quad (5)$$

where E_1 and E_2 are the modal fields and $\epsilon_m(x,y)$ is the m th component of the Fourier series of the perturbation, defined by

$$\begin{aligned} \epsilon(x,y,z) &= \epsilon_0(x,y,z) + \Delta\epsilon(x,y,z) \\ \Delta\epsilon(x,y,z) &= \sum_{m \neq 0} \epsilon_m(x,y) e^{-i(m K z)} \end{aligned} \quad (6)$$

where $\epsilon_0(x,y,z)$ is the unperturbed dielectric tensor.

The travelling perturbation gives rise to a frequency shift in the coupled light given by,

$$\omega_2 = \omega_1 + \frac{\beta_2 - \beta_1}{|\beta_2 - \beta_1|} m\Omega \quad (7)$$

where ω_2 and ω_1 are the optical frequencies associated with modes 1 and 2 of the fibre respectively and Ω is the angular frequency of the perturbing acoustic wave. If the perturbation is counter-propagating with respect to the light in the two modes, then the frequency shift is equal in magnitude but opposite in sign to that given in (7), hence an upshift becomes a downshift and vice versa.

Solving equations (1 and 2) with the initial conditions $A_1(0) = 1$ and $A_2(0) = 0$, that is, only one eigenmode populated at the start of the interaction region, yields the following solutions

$$\begin{aligned} A_1(z) &= e^{(i\Delta\beta z/2)} \left[\cos\alpha z - \frac{i\Delta\beta}{2} \sin\alpha z \right] \\ A_2(z) &= \frac{-i e^{(-i\Delta\beta z/2)} \kappa^* \sin\alpha z}{\alpha} \end{aligned} \quad (8)$$

where α is defined by

$$\alpha = \sqrt{|\kappa|^2 + \left(\frac{\Delta\beta}{2}\right)^2} \quad (9)$$

The fraction of power coupled from mode 1 to mode 2 in an interaction length z is thus defined by

$$P(z) = \left| \frac{A_2(z)}{A_1(0)} \right|^2 = \frac{|\kappa|^2}{|\kappa|^2 + \left(\frac{\Delta\beta}{2}\right)^2} \sin^2 \left(z \sqrt{|\kappa|^2 + \left(\frac{\Delta\beta}{2}\right)^2} \right) \quad (10)$$

Evidently, complete power transfer ($P(z) \equiv 1$) can only occur if $\Delta\beta \equiv 0$. This is known as the longitudinal phase matching condition and, from equation (3), this is equivalent to matching the spatial period of the perturbation Λ to the beat length associated with the two modes of the fibre.

$$\beta_1 - \beta_2 - mK = 0 \quad \text{hence} \quad \Lambda = \frac{2\pi}{K} = \frac{2\pi m}{|\beta_1 - \beta_2|} = m L_B \quad (11)$$

In most cases one need only consider the condition of $m=1$, however, it has been shown [11] that for flexural wave coupling of birefringence eigenmodes, the $m=2$ condition must be used.

With this condition satisfied equation (10) reduces to

$$P(z) = \sin^2(|\kappa|z) \quad (12)$$

Hence, 100% coupling may be achieved for an interaction length, L defined by

$$|\kappa|L = n\pi + \frac{\pi}{2} \quad (n = 0, 1, 2, \dots) \quad (13)$$

3.2 Beatlength determination.

The theory given above indicates that 100% power transfer between two coupled modes can only occur if the longitudinal phase matching condition has been satisfied. Hence, it is vital to know the beatlength associated with the two modes of interest. The accuracy of determination of the beatlength defines the tuning bandwidth required of the acoustic transducer used to generate the appropriate acoustic wave.

The beatlength of a highly birefringent fibre is one of the parameters supplied by the manufacturer. To check the manufacturer's figure, an experiment was performed to measure the birefringent beatlength. This was achieved by illuminating both eigenmodes with a fairly high power laser and then observing the Rayleigh scattered light exiting through the side of the fibre. Along the bisector of the eigenmode axes, a beat pattern is then clearly visible and has a spatial distribution equal to the beatlength. The beatlength could thus be measured directly with a travelling microscope. The highly birefringent fibre used in these experiments was supplied by York Technology (operation wavelength 633nm) and had a quoted beatlength of 1.3mm. The experimentally measured beatlength was 1.2 ± 0.05 mm.

The beatlength between the two lowest order spatial modes of a normal circular core optical fibre may be calculated from fibre parameters using the following equation [13],

$$L_B = 2 \pi a \left[\frac{2}{\Delta} \right]^{1/2} f(V) \quad (14)$$

where a is the fibre core radius, Δ is the normalised core-cladding refractive index difference and $f(V)$ (≈ 0.7 for V values of two-moded fibres) is a function of the normalised frequency. For a typical (nominally circular core) fibre, supplied by Lightwave Technology (operation wavelength 820nm, illuminated at 632.8nm) with $a = 2.75\mu\text{m}$, $V = 3.1$ and $\Delta = 0.003$, (14) gives a beatlength of $312\mu\text{m}$.

To confirm the correct spatial distribution for optimum coupling of the modes, pairs of ridged blocks, with the ridge spacing corresponding to the beatlengths determined above, were constructed and used to squeeze the fibre into a series of bends, thereby approximating a static flexure wave. As stated in section 3.1, for the birefringent fibre case, the spacing is twice the beatlength ($2 \times 1.2 = 2.4\text{mm}$ for the York 633nm fibre used). For the two-spatial moded case the spacing is simply equal to the beatlength (beatlength= $312\mu\text{m}$ for Lightwave Technology 820nm fibre used, illuminated at 632.8nm). To achieve a spacing of $312\mu\text{m}$, a wire with diameter $270\mu\text{m}$, was wrapped closely around a smooth block and the fibre was laid across the wire ridges at an angle of approximately 30° ($270/\cos 30^\circ = 312$). Optimal static coupling was confirmed for both devices.

3.3 Alignment of birefringence eigenaxes.

It is shown in references [6 and 11] that for the birefringent fibre it is necessary to align the plane of the perturbation (or plane of vibration for a flexure wave) to the plane of the bisector of the birefringence eigenaxes, in order to achieve optimal coupling. This must be achieved throughout the interaction length. If the plane of the perturbation is exactly aligned with either eigenaxis, then no coupling will occur. Hence, a method for orienting the optical fibre such that the plane of the eigenaxis bisector is known is essential.

The highly birefringent fibre used was of the 'bow-tie' variety. A method was developed (see figures 3-1 and 3-2) whereby the beam from a helium-neon visible laser was split into two beams with a cube beamsplitter, such that the two beams travelled parallel, but vertically separated and fractionally laterally separated with respect to each other. One beam was arranged to pass through the side of a short, vertical length of the stripped birefringent fibre which had been pre-aligned under a microscope (by observation of the bow-tie structure) such that the light travelled along the eigenaxis bisector. This gave rise to a diffraction pattern related to the spacing of the internal structure of the fibre. The second optical beam was arranged to traverse the stripped optical fibre of unknown eigenaxis alignment, which was allowed to hang freely. The diffraction pattern from this test fibre could be compared to that produced by the reference fibre and by rotating the test fibre, about the vertical axis,

the two patterns could be made identical. That point on the test fibre then has the same orientation as that known for the reference fibre. The method can be repeated at several points along the fibre to confirm the eigenaxis bisector orientation along its entire length.

3.4 Excitation of flexural acoustic waves on an optical fibre.

To excite flexural waves on optical fibres, transducers based on piezo-electric, thickness mode plates were attached to silica acoustic horns drawn from silica rod (c.f. Kim et al [5], see figure 3-3). The longitudinal acoustic waves produced by the piezo-electric plate are amplified by the gradual reduction of the acoustic horn diameter. The tip of the horn may then be attached to the side of an optical fibre and the longitudinal vibration of the tip excites bidirectional flexural acoustic waves, which travel away along the fibre.

3.5 Dispersion relations.

The acoustic dispersion relation relates the frequency and wavelength of an acoustic wave excited upon a particular structure. Using the dispersion relations given in the literature, the frequency of the flexural waves required to couple modes with the beatlengths ascertained above could be calculated. For a flexural acoustic wave excited on a thin rod of circular cross-section, the relation is given by [6],

$$\Omega = \frac{K^2 r}{2} \sqrt{\frac{E}{\rho}} \quad (15)$$

where Ω is the acoustic angular frequency, K is the acoustic wavenumber, r is the rod radius, E is the Young's modulus of the rod and ρ is its density.

To confirm the dispersion relation governing the frequency and wavelength of flexure waves on a thin rod (the optical fibre), for flexural

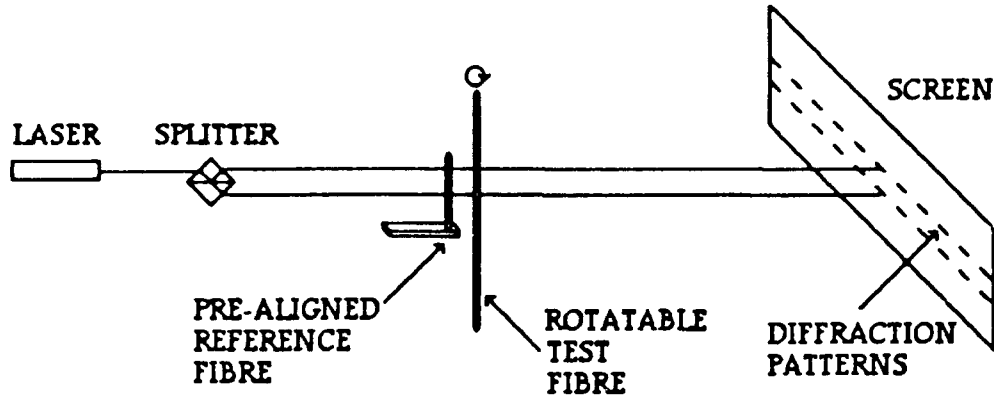


Figure 3-1 : (Bow-tie) Birefringence eigenaxis alignment.

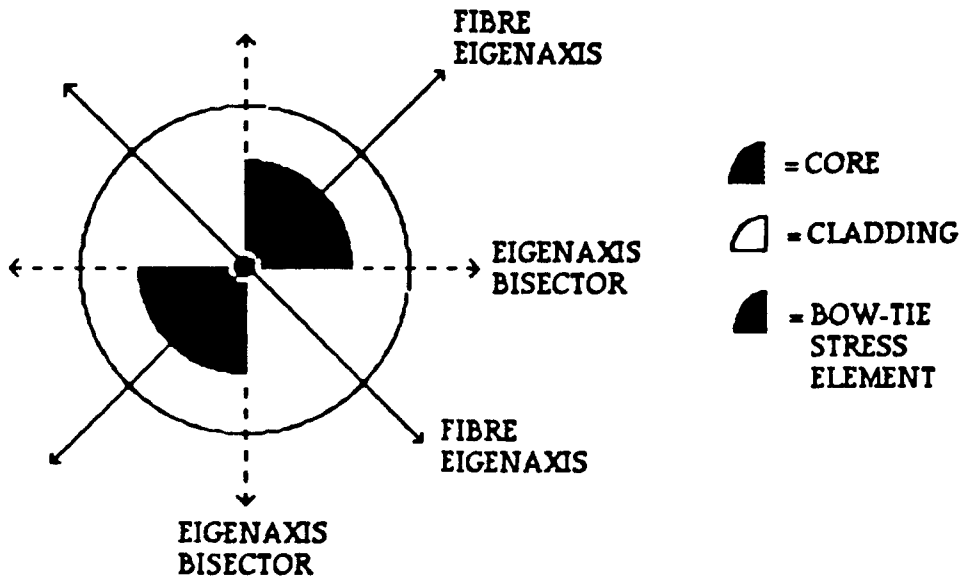


Figure 3-2 : Schematic of 'bow-tie' fibre cross-section.

wavelengths in the region of those required for a birefringent fibre shifter, a small length of silvered (York bow-tie highly birefringent 633nm fibre) optical fibre was attached to the tip of a flexure wave transducer acoustic horn (see figure 3-4). Standing flexural acoustic waves were set up on the fibre by varying the drive frequency applied to the piezo-electric plate. The relative amplitude of these vibrations was measured, using the heterodyne vibrometer, as a function of distance along the fibre (see figure 3-5). Hence the spacing of minima, and thus the wavelength of the acoustic wave, were measured. This was carried out for a number of frequencies such that the dispersion relation could be confirmed. This method was used to confirm the relation in the region of wavelengths from 2-3mm (see figure 3-6).

3.6 Flexural acoustic wave fibre frequency shifter.

A length of stripped birefringent fibre (stripped section length approximately 25cm) was oriented in the manner described in section 3.3, and a flexure wave transducer, designed to operate at 195kHz (equivalent flexural wavelength= 2.4mm) was attached by fusing the tip of the acoustic horn to the side of the fibre using silica jointing paste and a small oxy-propane torch. With one eigenmode populated, this device constituted a flexural acoustic wave fibre frequency shifter, and was incorporated into one arm of a heterodyne Mach-Zehnder interferometer in order to investigate its performance. The frequency spectrum of the detector output was observed with a spectrum analyser. No definite frequency shift (identifiable as a single 'sideband' at a frequency twice the drive frequency away from the Bragg cell 'carrier' frequency of 40MHz) was observed, although a high degree of phase modulation of the guided light (characterised by symmetric sidebands, at the drive frequency and harmonics thereof about an 40MHz carrier) was observed with high drive powers (see figure 3-7). Additional acoustic damping at the fibre ends was incorporated by applying silica rubber compound, to ensure that the double sidebands were not a consequence of standing waves being set up on the fibre. This indicated that the acousto-optic interaction was either not properly phase matched or that the interaction strength was insufficient for observation of a shifted component. Several similar

devices were constructed to confirm that the transducer/fibre joint was not at fault, but no improvement was obtained.

This result would appear to be at variance with the results reported by Pannell et al [6,11]. One must first realise that this work was carried out taking the longitudinal phase matching condition to be that the flexural acoustic wavelength must equal twice the birefringent beatlength, whereas the work of [6] used the condition of equal wavelength and beatlength. The theoretical analysis presented in [11] shows the former phase matching condition to be the more favourable. If this is indeed the case, then the flexural wave amplitude generated in the prototype device presented in this work, must indeed have been insufficient to couple a significant proportion of the optical power.

Piezo-electric thickness-mode transducers were not available at the frequency required to repeat the work of [6] and, as presented in the remainder of this report, an improved method for coupling the polarisation modes of a highly linearly birefringent fibre was developed.

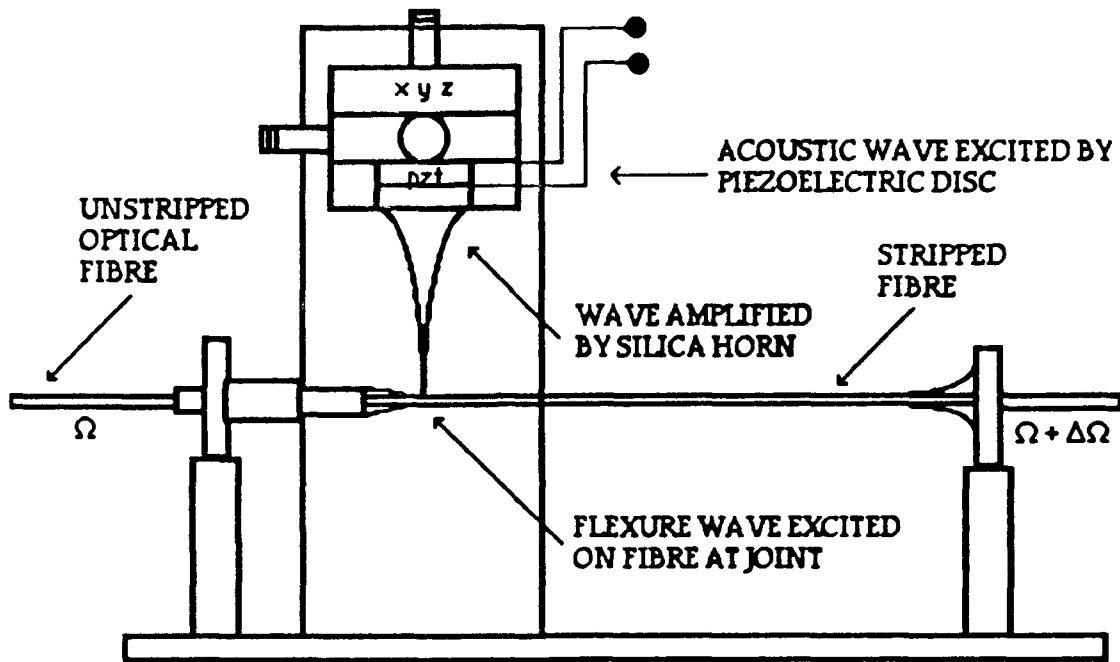


Figure 3-3 : Schematic of flexural acoustic wave fibre frequency shifter.

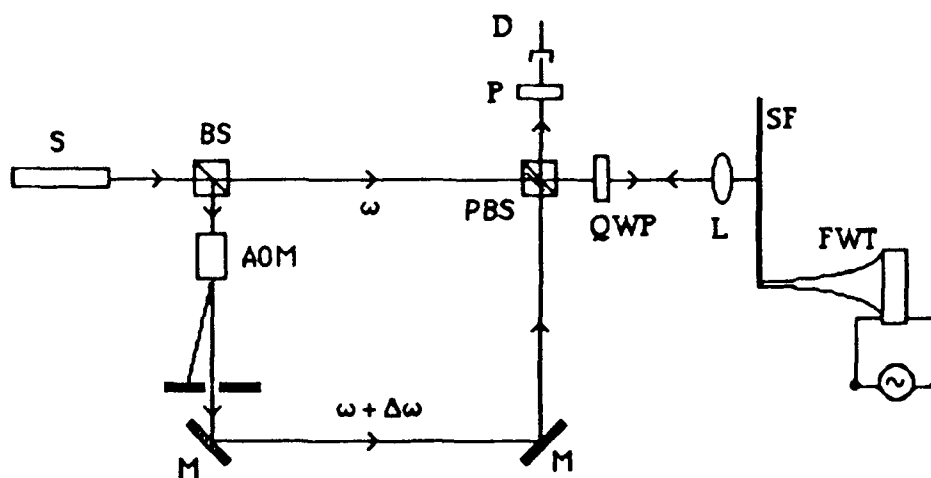


Figure 3-4 : Schematic of flexural wavelength measurement.

[S : laser source, BS : beamsplitter, AOM : acousto-optic modulator (40MHz Bragg cell), M : mirror, PBS : polarising beamsplitter, QWP : quarter waveplate, P : polariser, D : detector, L : lens, SF : silvered fibre, FWT : flexural wave transducer]

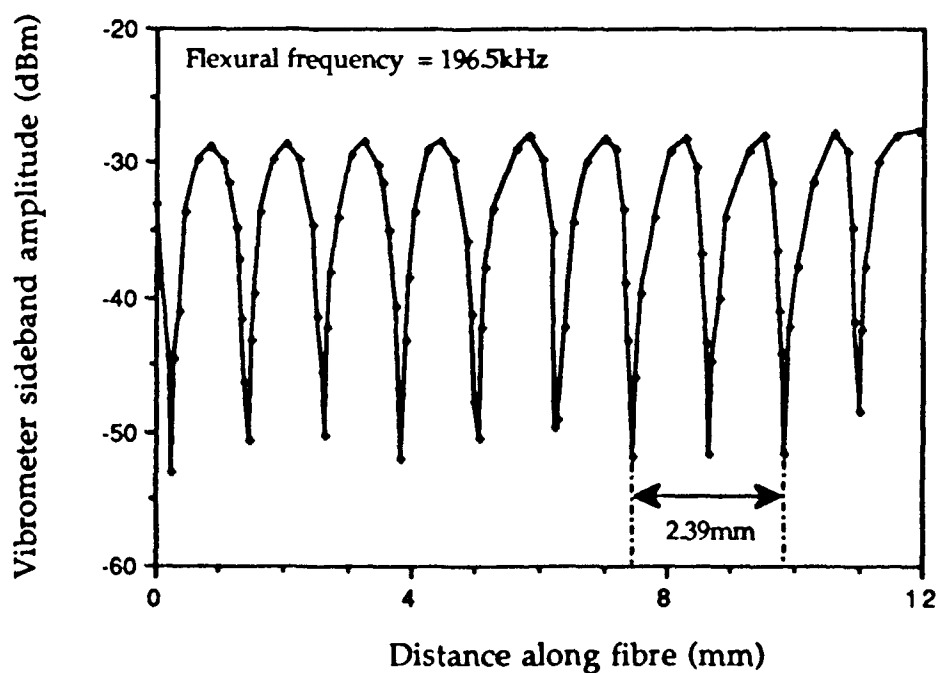


Figure 3-5 : Vibration amplitude as a function of distance along fibre.

[Fibre diameter = 123 μ m]

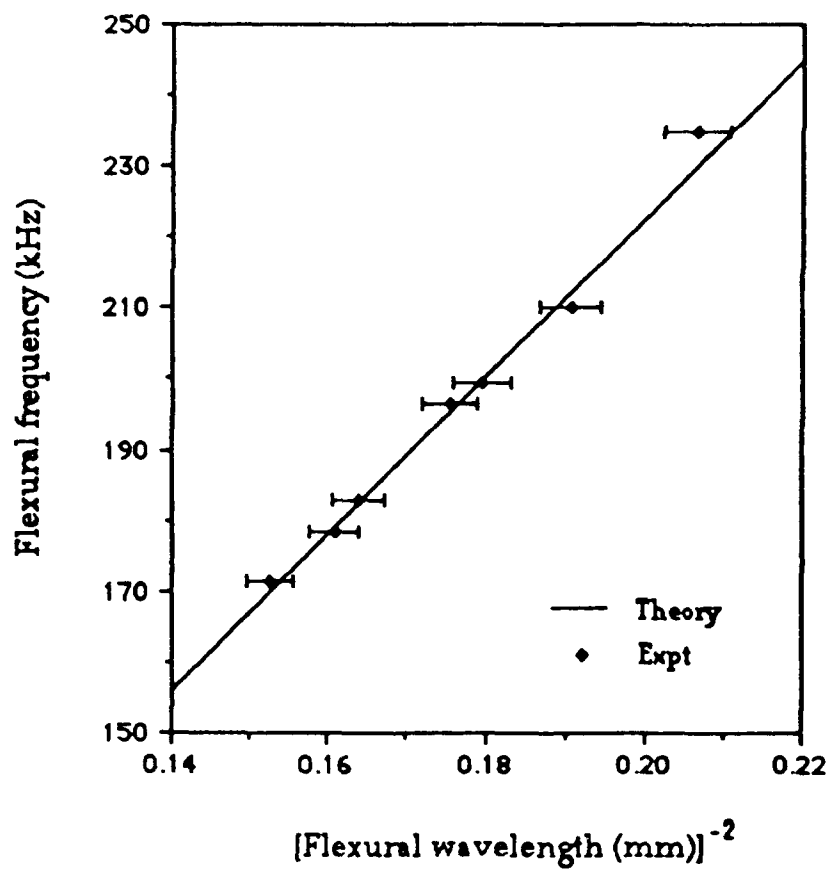
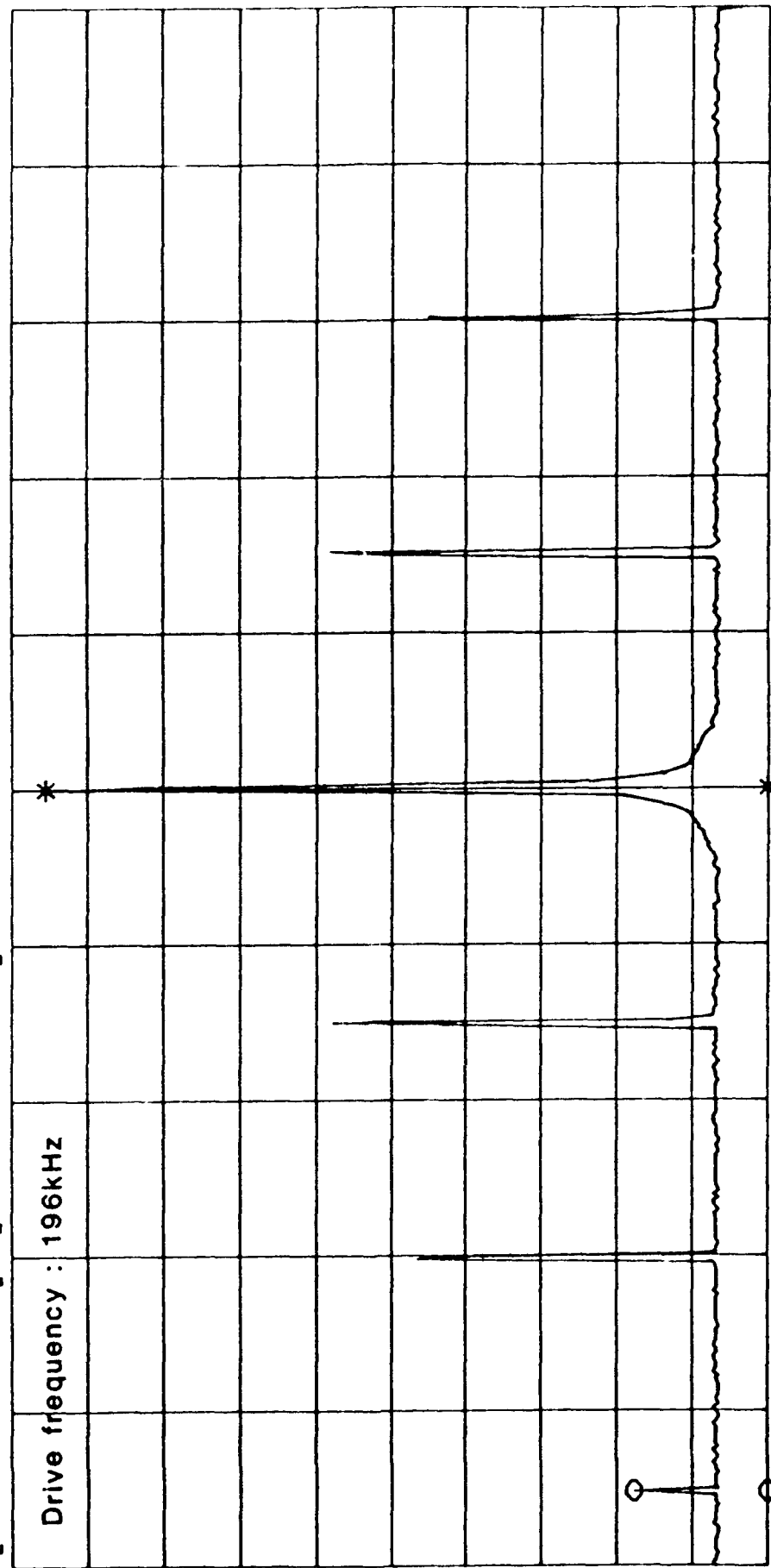


Figure 3-6 : Plot of experimental and theoretical dispersion relation for flexural waves excited on an optical fibre.

SPECTRUM Math AVERAGING 32
 A: REF B: REF Δ MKR 588 250.000 HZ
 -42.51 0.000 ΔMAG 62.1084 dB
 [dBm] [ΔMAG]



DIV 8.000 DIV 10.00 CENTER 39 997 500.000 HZ
 RBW: 1 KHZ ST: 20.5 sec SPAN 1 300 000.000 HZ
 RANGE: R=-40, T=-20dBm

Figure 3-7

Due to the poor performance achieved with the initial design of the fibre frequency shifter, a more detailed analysis was undertaken which showed that the use of flexure waves to couple the birefringent axes is non-ideal. This is because the coupling is the result of rotation of the local birefringence eigenaxes, which is essentially a second order effect of the bending induced by the flexure waves and yields a very poor coupling coefficient. A better method for coupling the birefringent modes is to produce rotations directly by exciting a travelling torsional acoustic wave on the fibre. It is shown in section 4 that this method of birefringent fibre perturbation gives a much improved coupling coefficient; also for a typical birefringent fibre with a beatlength of 1.2mm the torsional wave frequency is approximately 3MHz as opposed to 195kHz for a flexural wave. This higher frequency is much more useful for general signal processing as it allows higher bandwidth signals. The generation of torsional waves on an optical fibre to effect a frequency shift is a novel concept.

The simplest configuration for such a shifter requires two silica acoustic horns, joined to opposite sides of the fibre and excited in phase (see figure 3-8). However, bonding the two horns and the fibre was expected to give rise to a large structure (relative to the fibre diameter), with built-in stresses which could lead to rapid failure of the joints. An alternative configuration (see figure 4-1) relies on fusing a small length of fibre at right angles to the main fibre (this can be achieved with a commercial fusion splicer). A flexure wave is then excited on this side-fibre, using a silica horn, which gives rise to travelling torsional and flexural waves on the main fibre. Torsional and flexural waves have different propagation velocities, hence if the torsional wavelength is matched to the fibre beatlength, then the flexural wave will be unmatched. To increase the useful torsional acoustic wave amplitude, a second side-fibre positioned a quarter of an acoustic wavelength along the fibre and driven $\pi/2$ out of phase with the first, should serve to reinforce the torsional wave travelling in one direction along the fibre, cancel the torsional wave travelling in the opposite direction and provide some degree of filtering of the flexural wave. This configuration was constructed and tested and is reported in section 4.

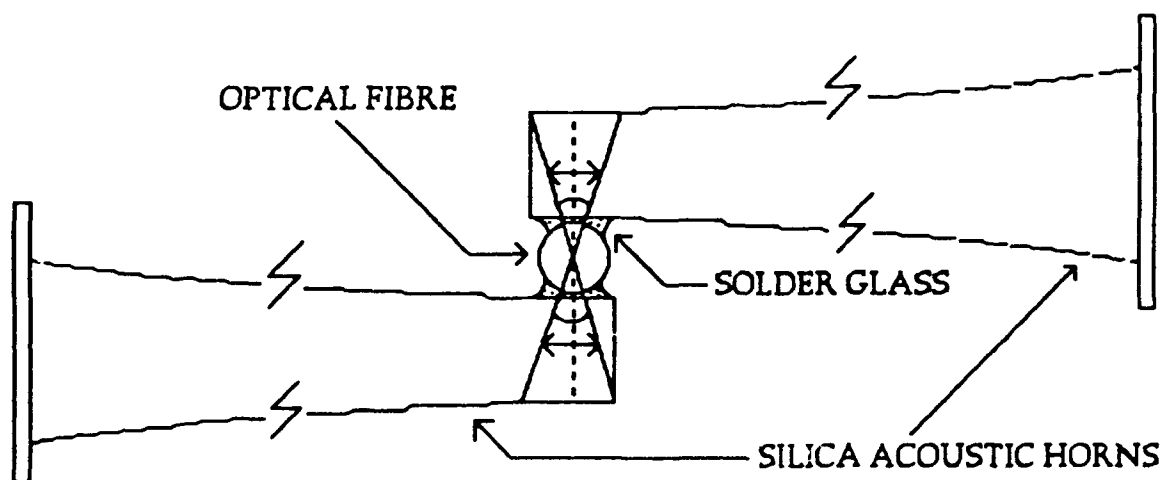


Figure 3-8 : Simple torsional transducer

4 Torsional acoustic wave highly birefringent fibre frequency shifters.

4.1 Introduction

The work presented below is an analysis of the use of torsional acoustic waves, excited upon an optical fibre, to couple light from one birefringent axis of the fibre to the other; imparting a frequency shift to the coupled light. Torsional wave generator designs are presented in sections 4.3 and 4.4, along with experimental results for fibre frequency shifters based on these designs.

4.2 Theoretical analysis.

4.2.1 Dispersion relation for torsional waves.

Assume the optical fibre has cylindrical symmetry, with a circular cross-section radius a_f .

The wave equation for torsional waves may be written,

$$C \frac{\partial^2 \Phi}{\partial z^2} = \rho I \frac{\partial^2 \Phi}{\partial t^2} \quad (16)$$

where ρ is the density of the fibre, I is the moment of inertia of the cross-section about the centre of mass and C is the torsional rigidity given by

$$C = \frac{1}{2} (G \pi a_f^4) \quad (17)$$

where G is the modulus of rigidity or shear modulus, given by

$$G = \frac{E}{2(1 + \sigma)} \quad (18)$$

where E is the Young modulus of the fibre and σ is the Poisson ratio.

$$I = \int (x^2 + y^2) dS$$

$$I = \int_0^{2\pi} \int_0^{a_f} r^2 r dr d\theta = 2\pi \int_0^{a_f} r^3 dr = \frac{\pi a_f^4}{2} \quad (19)$$

Hence, torsional wave propagation velocity, v_t , is given by

$$v_t = \sqrt{\frac{C}{\rho I}} = \sqrt{\frac{E}{2(1+\sigma)\rho}} \quad (20)$$

This velocity is clearly independent of wavelength, in contrast with the flexural wave velocity for a similar fibre, given by

$$v_f = \frac{v_l}{\sqrt{1 + \left\{ \frac{\lambda_f}{\pi a_f} \right\}^2}} \quad (21)$$

where v_l is the longitudinal wave velocity given by

$$v_l = \sqrt{\frac{E}{\rho}} \quad (22)$$

Hence, for the following fibre parameters the torsional wave velocity may be calculated.

$$E = 73 \times 10^9 \text{ Pa} , \rho = 2.20 \times 10^3 \text{ Kgm}^{-3} , \sigma = 0.17$$

$$v_t = 3.77 \text{ kms}^{-1}$$

Hence, for a highly birefringent monomode fibre with cladding diameter ($2a_f$) of $125\mu\text{m}$ and a beat length (LB) of $1.2 \pm 0.05 \text{ mm}$, the acoustic

frequency corresponding to the acoustic wavelength which matches the beat length (i.e. the dispersion relation) is simply

$$v_t = \frac{v_t}{\lambda(=LB)} = 3.14 \pm 0.13 \text{ MHz}$$

this may be compared to the flexural wave frequency required for this fibre

$$v_f = \frac{v_f(\lambda)}{\lambda(=2LB)} = \frac{0.47 \pm 0.02 \text{ kms}^{-1}}{2 \times 1.2 \pm 0.05 \text{ mm}} = 0.20 \pm 0.02 \text{ MHz}$$

4.2.2 Derivation of torsional wave coupling coefficient for highly birefringent fibre

Utilising the coupled mode theory given in section 3.1, an expression for the torsional wave coupling coefficient may be derived as follows (c.f. derivation for flexural wave coupling , chapter VI of reference [11]).

Assume the fast and slow eigenaxes of the fibre are taken to coincide with the x,y coordinate system axes. Working in a co-moving frame so that equations (1-6) contain no explicit time dependence. Furthermore assume that the coupling perturbation takes the form of a torsional wave which exists on the fibre and has a peak angular displacement Θ . Hence the rotation of the eigenaxes may be written as

$$\theta = \Theta e^{-i K z} \quad (23)$$

and comparison with equation 6 shows that only the m=1 terms are significant. Utilising Jones matrix notation, the unperturbed dielectric tensor is given by

$$\epsilon_0(x,y,z) = \epsilon_0 \begin{bmatrix} n_1^2 & 0 \\ 0 & n_2^2 \end{bmatrix} \quad (24)$$

where n_1 and n_2 are the refractive indices of the two modes of the fibre. Then,

$$\begin{aligned} \Delta\epsilon(x,y,z) &= \epsilon_0 \left\{ \begin{bmatrix} \cos\theta & \sin\theta \\ -\sin\theta & \cos\theta \end{bmatrix} \begin{bmatrix} n_1^2 & 0 \\ 0 & n_2^2 \end{bmatrix} \begin{bmatrix} \cos\theta & -\sin\theta \\ \sin\theta & \cos\theta \end{bmatrix} \begin{bmatrix} n_1^2 & 0 \\ 0 & n_2^2 \end{bmatrix} \right\} \\ &= \epsilon_0 (n_1^2 - n_2^2) \begin{bmatrix} \sin^2\theta & \sin\theta\cos\theta \\ -\sin\theta\cos\theta & -\sin^2\theta \end{bmatrix} \end{aligned} \quad (25)$$

as θ is small, (25) becomes

$$\Delta\epsilon(x,y,z) = \epsilon_0 (n_1^2 - n_2^2) \begin{bmatrix} 0 & \theta \\ \theta & 0 \end{bmatrix} \quad (26)$$

From (23), only the $m=1$ term of the perturbation is retained, hence

$$\epsilon_1(x,y,z) = \epsilon_0 (n_1^2 - n_2^2) \begin{bmatrix} 0 & \theta \\ \theta & 0 \end{bmatrix} \quad (27)$$

The modal fields of the two eigenmodes of the fibre may be taken to be transverse and identical except for polarisation. Hence they may be written as,

$$\begin{aligned} E_1 &= \chi \begin{bmatrix} 1 \\ 0 \end{bmatrix} f(x,y) \\ E_2 &= \chi \begin{bmatrix} 0 \\ 1 \end{bmatrix} f(x,y) \end{aligned} \quad (28)$$

where $\begin{bmatrix} 1 \\ 0 \end{bmatrix}$ and $\begin{bmatrix} 0 \\ 1 \end{bmatrix}$ are the Jones vectors for vertical and horizontal linearly polarised states (i.e. linear states aligned to the x-y axes) and χ is a normalisation constant. In arriving at equations (1-6), the following normalisation condition has been used

$$\langle i | j \rangle \equiv \iint E_i^* E_j dA = \frac{2\mu\omega}{|\beta_i|} \delta_{ij} \quad (29)$$

This includes the orthogonality of the modes and defines unitary power flow. The coupling constant $\kappa^{(1)}$ may now be derived from equations (5,27,28)

$$\kappa^{(1)} = \frac{\omega}{4} \iint \left(\chi \begin{bmatrix} 1 \\ 0 \end{bmatrix} \right)^* f(x,y) \left(\epsilon_0 (n_1^2 - n_2^2) \begin{bmatrix} 0 & \Theta \\ \Theta & 0 \end{bmatrix} \right) \chi \begin{bmatrix} 0 \\ 1 \end{bmatrix} f(x,y) dA$$

$$\kappa^{(1)} = \frac{\chi^2 \omega \epsilon_0}{4} \Theta (n_1^2 - n_2^2) \iint f(x,y)^2 dx dy \quad (30)$$

from equation (29)

$$\chi^2 \iint f(x,y)^2 dx dy = \frac{2\mu\omega}{|\beta|}$$

thus

$$\kappa^{(1)} = \frac{\omega^2 \mu \epsilon_0 \Theta (n_1^2 - n_2^2)}{2 k_0 n_1} \quad (31)$$

where $k_0 = \frac{2\pi}{\lambda}$ is the free space optical wavenumber, λ is the wavelength and $|\beta| \sim k_0 n_1$ ($\sim k_0 n_2$) introduces very little error. Substituting for the permeability $\mu \approx \mu_0$,

$\mu_0 \epsilon_0 = \frac{1}{c^2}$, where c is the speed of light, and $\frac{\omega^2}{c^2} = k_0^2$, equation (31) becomes

$$\kappa^{(1)} = \frac{k_0 \Theta (n_1 + n_2)(n_1 - n_2)}{2 n_1} \approx k_0 \Theta (n_1 - n_2) \quad (32)$$

The beat length of the fibre is given by

$$L_B \equiv \frac{2\pi}{|\beta_1 - \beta_2|} \approx \frac{2\pi}{k_0 (n_1 - n_2)} \quad (33)$$

hence the coupling constant is simply given by

$$\kappa^{(1)} = \frac{2\pi \Theta}{L_B} \quad (34)$$

c.f. the coupling constant for flexural wave coupling

$$\kappa^{(2)} = \frac{n^3(p_{12} - p_{11})(1 + \sigma) d^2 a^2 K^4 k}{16} \quad (35)$$

where p_{12} and p_{11} are components of the strain optic tensor (= 0.27 and 0.12 respectively for silica) n is the refractive index of the fibre (= 1.46) and d is the amplitude of the fibre displacement.

Equating (13 and 34) gives the angular displacement required for complete coupling

$$\Theta(100\%) = \left(\frac{L_B}{4L} \right) \quad (36)$$

For example, if $L_B = 1.2$ mm and $L = 50$ cm then $\Theta(100\%) = 0.6$ mrad, which corresponds to a peak surface displacement of 37.5 nm (assuming fibre radius = 62.5 μm).

c.f. from equations (13 and 35) displacement of flexural wave for 100% coupling

$$d(100\%) = \frac{\pi}{2L} \frac{16}{n^3(p_{12} - p_{11})(1 + \sigma) a^2 K^4 k} \quad (37)$$

for the same length of similar fibre $d = 7.1$ μm , that is ~190 times greater than for the torsional wave.

4.3 Torsional wave hibi fibre frequency shifter I : 'Side-fibre' configuration.

4.3.1 Generation of torsional acoustic waves.

The first configuration utilised for the generation of torsional waves on an optical fibre and its mode of operation are shown in figures 4-1,4-2 and 4-3. The configuration consists of a small length of fibre joined to the main fibre at right angles; joint 1. A flexural wave is then excited on this side fibre, using a piezoelectric plate resonator and silica horn acoustic amplifier, attached at the distal end of the side-fibre; joint 2. At joint 1 the

flexural wave gives rise to bidirectional, travelling, torsional waves on the main fibre (figure 4-2). A second torsional wave generator, positioned a quarter of an acoustic wavelength along the fibre (joint 3) and driven $\pi/2$ out of phase with the first, also generates bidirectional waves on the main fibre. The relative phase of the two pairs of codirectional torsional waves at joints 1 and 3, reinforce the torsional wave travelling in one direction along the fibre and cancel the torsional wave travelling in the opposite direction (figure 4-3).

The main advantage of using torsional, rather than flexural, waves to couple the birefringent axes, is the greatly increased interaction strength, as shown above. However, an additional advantage may be exploited; in the orientation of the fibre with respect to the acoustic drive. In the flexural wave case, for optimum coupling, the plane of the transverse vibration of the flexural waves must be aligned with the direction of the bisector of the fibre eigenaxes. This condition must be satisfied, not only at the joint of the silica horn excitor, but along the full length of the interaction region. Techniques have been developed to achieve this alignment; based upon the comparison of the diffraction patterns obtained by side-illumination of the fibre and a reference fibre of known eigenaxis orientation. However, this is a point alignment technique and must be carried out at several points along a given length of the fibre. This is unnecessary for torsional waves as the vibration is circumferential rather than transverse. Furthermore, the joining of a silica horn or side fibre inevitably gives rise to some static stress within the fibre. Joining at 45° to the fibre eigenaxes, as in the flexural case, is optimal for coupling the eigenaxes and hence the static stress gives rise to a maximum degree of undesirable static coupling of the modes. In the torsional case it is both desirable and permissible to join the side-fibre at a point directly in line with one of the eigenaxes, giving a minimum of static coupling. The attachment of the torsional wave generator side fibres along a birefringence eigenaxis was not possible within the present configuration, as the use of the commercial fusion splicer prevented access for alignment of the axes. A new method for fusing the silica joints, which utilises an electrical arc generated by freely accessible electrodes has been developed, allowing fused joints to be made in the manner described above.

4.3.2 Experimental

The 'main fibre' utilised in the experiments was a York Technology highly linearly birefringent monomode optical fibre of outer diameter 125 microns. The side fibres were short lengths of the same fibre, and were joined to the main fibre using a commercial fusion splicer (BICC AFS3100) modified by the addition of a micropositioner to permit alignment of the side-fibres at right-angles to the main fibre, prior to fusing. The beatlength of the main fibre was measured using the method of section 3.2, and found to be $L_B = 1.2 \pm 0.05$ mm. In order to match the wavelength of the torsional wave to this beatlength it was necessary to generate a torsional wave at a frequency of 3.14 ± 0.14 MHz.

The piezoelectric resonator/silica horn arrangement is shown in figure 4-2. It consisted of a piezoelectric plate (12x12x0.5mm) poled for thickness resonance at a frequency of 3 MHz (that is, at the resonant frequency, the thickness of the plate equals half a wavelength for longitudinal acoustic waves propagating in the piezoelectric material). This was attached to an aluminium backing plate, as shown. The thickness of the aluminium backing was also designed to be half a longitudinal wavelength, forming a resonant cavity, which enhanced the forward propagating wave. The piezoelectric plate was attached using conductive (silver loaded) paint. A silica acoustic horn was attached to the other side of the piezoelectric plate using a thin layer of epoxy adhesive (Araldite). Electrical connections were made to the top and bottom of the piezoelectric plate by soldering and conductive paint respectively.

The silica horns were formed by drawing down short lengths of 4 mm diameter silica rod, on a glass lathe, to a tip diameter of $\approx 300\mu\text{m}$. The tips of the silica horns were joined at 90° to the ends of the side fibres using a low melting point, silica jointing paste (American Vitta Corporation type P-1015) and an oxy-propane microtorch. It was not possible to fuse this joint using the fusion splicer due to the inaccessibility of the electrodes.

The torsional wave generator described above formed the basis of a frequency shifter and was incorporated into one arm of a Mach-Zehnder interferometer for evaluation. The highly birefringent fibre was supported such that the device comprised a total interaction length of 600 mm of

fibre stripped of its plastic buffer coating, bounded by lengths of unstripped fibre, with the coating acting as acoustic absorbers at either end of the interaction region. The interferometric test configuration is shown in figure 4-4. The optical source was a helium-neon laser operating at a wavelength of 632.8 nm. The light from this source passed through a Glan-Thompson prism polariser to ensure a highly linearly polarised optical state and was then amplitude divided by the beamsplitter. One beam passed through a halfwave plate before being launched into the prototype fibre frequency shifter fibre. The waveplate was rotated so as to populate only one eigenaxis of the fibre (slow axis, say), the torsional wave excited by the acoustic transducer then coupled light to the other eigenmode (fast axis) imparting a frequency shift $\Delta\nu$. The ejected light from the fibre was collimated and passed through a second Glan-Thompson prism polariser, oriented to filter the shifted light from the unshifted light, remaining in the first eigenmode. The reference path beam traversed a bulk acousto-optic frequency shifter (Bragg cell) which imparted a 40 MHz shift. This light then passed through a halfwave plate and polariser oriented to give a linear state of the same azimuth as the shifted light. The two beams were then recombined at a second beamsplitter and mixed on the surface of an avalanche photodiode.

The frequency spectrum of the output from the detector was investigated using a spectrum analyser (Hewlett Packard hp4195A). For the ideal case of zero static coupling and 100% dynamic coupling by a monodirectional wave fibre shifter, a single frequency component at 40 MHz - $\Delta\nu$ (slow \rightarrow fast axis coupling = downshift) would be generated. In practise a heterodyne carrier component, at the Bragg cell frequency, with upshifted and downshifted components corresponding to the fibre frequency shifter is found. The carrier frequency is present due to static coupling of the eigenmodes and the second sideband derives from the bidirectional generation of the coupling acoustic waves. The degree of suppression of the two unwanted components, along with the efficiency of generation of the desired shifted component, are measures of the overall performance of the device.

4.3.3 Results

Initially, only one of the two torsional wave generators was driven. The drive electronics consisted of a signal generator (Hewlett Packard HP8656B) producing a sinusoidal output, initially at 3 MHz, which was amplified and fed to the piezoelectric plate resonator via an impedance matching circuit. The spectral output from the detector, as viewed on the spectrum analyser, was seen to contain the three components described above. The prominent component was the upshifted frequency, hence coupling was occurring from the fast axis to the slow axis. Rotation of the input azimuth by 90° produced a prominent downshifted component corresponding to coupling from the slow axis to the fast axis. Optimisation of the coupling, by varying the drive frequency to more accurately match the torsional wavelength to the fibre beatlength, gave an optimal drive frequency of 3.195 MHz.

Fig 4-5(a) shows a spectrum analyser trace corresponding to the upshifting case, and fig 4-5(b) shows a trace corresponding to the downshifting case. The maximum amplitude of the downshifted signal, with the system optimised to measure the shifted light, was compared to the amplitude of the 40MHz carrier signal, when the system was optimised to measure the direct (uncoupled) throughput with no signal applied to the torsional wave generator. The maximum coupling efficiency was found to be 6% with an electrical drive power of 780mW to the transducer. This may be increased in a number of ways. Simply increasing the drive power is undesirable due to the problem of dissipation of heat produced at the piezoelectric mount. Continuous running of the transducer at drive powers of approximately 500mW produced a temperature increase of around 40° C. A second method of increasing the coupling efficiency would be to increase the interaction length. As the interaction length is already \approx 55 cm this option is also undesirable, indeed it would be preferable to decrease the interaction length if possible. The third option is to make more efficient use of the acoustic power which is being generated. This is discussed in detail below.

The final method is to utilise multiple torsional wave generators, spaced along the fibre, and operated with suitable phase delays, such as to reinforce the wave in one direction and reduce the wave in the opposite direction. Hence, the unwanted sideband suppression is also improved.

This possibility was investigated by driving both of the torsional wave generators, attached to the main fibre, simultaneously. The signal generator output formed the input to both sets of drive electronics and an electronic phase shifter was incorporated to enable the phase difference between the drive signals to be correctly adjusted, and hence the phase difference between the torsional waves produced by each generator, to be varied (attainable shift = $\pm 75^\circ$). The two generators were driven with equal drive power and the phase was varied over the full range available. The amplitudes of the three spectral components were somewhat unstable. The wanted (downshifted) sideband was the most stable (± 1 dB), the unwanted (upshifted) sideband was less stable (± 3 dB) and the carrier component was the least stable, fluctuating by up to 20 dB. It was possible to increase the downshifted sideband amplitude by (+)4.2 dB over the level obtained with only one generator driven, and to decrease the amplitude by (-)2.5 dB. For the same conditions, the upshifted sideband amplitude varied by +2.1 dB and -7.5 dB. The theory predicts that when one sideband is increased, the other should decrease, and that the maximum variation for equal wave amplitudes is ± 3 dB. The effects observed demonstrate that the coupling can be increased by adding a second generator, however they do not demonstrate the expected cancelling of the backward propagating wave. Furthermore, an increase of greater than 3 dB was obtained, hence the effect of the two generators exceeds the simple superposition of two waves. A possible explanation of this is the interaction of multiple waves within the region between the two side fibres produced by reflections from the joints. Optimisation of the matching of acoustic impedances throughout the configuration, as discussed below, is expected to improve this situation.

4.3.4 Acoustic power transfer analysis

This section will consider the transfer of acoustic power between the three types of acoustic waves which are generated within the fibre shifter configuration. That is, conversion of the acoustic power of the longitudinal wave in the silica horn tip to the flexural wave on the side fibre, and then to the torsional wave on the main fibre.

Following the method of Engan et al [12], rough estimates for the power transmission coefficients pertaining to these conversions will be given. These will be used to determine the efficiency of utilisation of the acoustic power generated by the piezoelectric plate/silica horn, and how this may be optimised.

A one-dimensional description of the forces in the fibres and silica horn tip, at each of the joints, is envisaged by replacing all distributed forces of a cross-section by a combined, localised force. With this model, standard transmission line theory gives expressions for the power transmission coefficients at each of the joints, as follows.

It is necessary to define the acoustic impedances of the longitudinal wave at the horn tip Z_t , the flexural wave on the side fibre Z_s , and the torsional wave on the main fibre Z_f .

$$Z_t = c_{\text{long}} \rho_t A_t \quad (38)$$

$$Z_s = c_{\text{flex}} \rho_s A_s \quad (39)$$

$$Z_f = c_{\text{tors}} \rho_f 2A_f \quad (40)$$

where, subscripts $i = t,s,f$ refer to the horn tip, side fibre and main fibre respectively, ρ_i are densities and A_i are cross-sectional areas. c_{long} , c_{flex} and c_{tors} are the longitudinal, flexural and torsional wave velocities respectively. The area A_f is counted twice because of the bidirectional excitation of the torsional waves. Assuming equal densities and cylindrical symmetry throughout, then

$$\rho_t = \rho_s = \rho_f = \rho \quad (41)$$

$$A_i = \pi (a_i)^2 \quad (42)$$

where a_i are radii. The power transfer coefficients may thus be written as

$$T_1 = T_{(\text{tlong} \rightarrow \text{sflex})} = \frac{4 Z_t Z_s}{(Z_t + Z_s)^2} \quad (43)$$

$$T_{2\pm} = T_{(\text{sflex} \rightarrow \text{ftors}\pm)} = \frac{2 Z_s Z_f}{(Z_s + Z_f)^2} \quad (44)$$

T_1 has a maximum value of 1, corresponding to complete power transfer, however, $T_{2\pm}$ has a maximum value of 0.5, taking into account the bidirectional excitation of torsional waves. Hence, T_{2+} and T_{2-} represent coupling to the forward and backward propagating waves respectively. Optimum transmission occurs when $Z_t = Z_s$ and $Z_s = Z_f$. This condition corresponds to

$$a_t = a_s \sqrt{\frac{c_{\text{flex}}}{c_{\text{long}}}} \quad (45)$$

$$a_s = a_f \sqrt{\frac{2c_{\text{tors}}}{c_{\text{flex}}}} \quad (46)$$

The overall power transfer efficiency, T , may now be calculated using the following figures : for silica : $c_{\text{long}} = 5.76 \text{ kms}^{-1}$, $c_{\text{tors}} = 3.77 \text{ kms}^{-1}$, $a_t = 150 \mu\text{m}$, $a_s = 62.5 \mu\text{m}$, $a_f = 62.5 \mu\text{m}$, $n = 3.195 \text{ MHz}$, hence , $\lambda(\text{flex}) = 579 \mu\text{m}$, $c_{\text{long}} = 1.85 \text{ kms}^{-1}$. Then from equations (38 - 44)

$$Z_t = 0.09 ; Z_s = 0.05 ; Z_f = 0.20$$

$$T_1 = 0.2 ; T_{2\pm} = 0.32 ; \text{ hence, } T = T_1 T_{2\pm} = 0.064 \text{ i.e. } 6.4\%$$

The calculations above assume that the only vibrational mode excited on the main fibre is the torsional mode (case 1). Consider the case where the joint between the main fibre and the side fibre does not occur at a node in the side-fibre flexural wave pattern, then a flexural wave will also be excited on the main fibre. This will not lead to coupling of the eigenmodes as the flexural wavelength will not be matched to the fibre

beatlength. However, this does represent a source of acoustic power loss to the torsional wave. Using the above formalism and assuming the case of equal excitation of both torsional and flexural waves on the main fibre (case 2), gives the following values for power transfer.

$$Z_{f(\text{tors})} = Z_f = 0.2 ; \quad Z_{f(\text{flex})} = c_{\text{flex}} \rho 2A_f = 0.1 \quad (47)$$

$$Z_f = Z_{f(\text{flex+tors})} = \frac{Z_{f(\text{tors})} Z_{f(\text{flex})}}{Z_{f(\text{tors})} + Z_{f(\text{flex})}} = 0.067 \quad (48)$$

$$\Gamma = T_1 T_{(s\text{flex} \rightarrow f(\text{tors+flex})\pm)} = T_1 \frac{2 Z_s Z_f}{(Z_s + Z_f)^2} = 0.197 \times 0.49 = 0.097 \quad (49)$$

hence, overall efficiencies of coupling to the torsional and flexural waves are given by

$$T(\text{tors})\pm = \frac{Z_{f(\text{flex})}}{Z_{f(\text{tors})} + Z_{f(\text{flex})}} \quad \Gamma = 0.032, \text{ i.e. } 3.2\% \quad (50)$$

$$T(\text{flex})\pm = \frac{Z_{f(\text{tors})}}{Z_{f(\text{tors})} + Z_{f(\text{flex})}} \quad \Gamma = 0.066, \text{ i.e. } 6.5\% \quad (51)$$

The exact alignment of the experimental system probably lies somewhere between the two cases given above, however when one takes into account the possible acoustic losses due to imperfect joints, then the overall power transfer to the useful torsional wave in the present system must be assumed to be only a few percent out of the possible 50%. Improvement of this figure is possible, by designing the dimensions of the components of the shifter configuration in line with the conditions given in equations (45 and 46). Given a main fibre radius of $= 62.5 \mu\text{m}$ and beatlength $= 1.2 \text{ mm}$, the side fibre and horn tip radii for optimum power transfer may be calculated.

Optimise for case 1:

$$a_s = 110 \mu\text{m} \text{ and } a_t = 71 \mu\text{m} \rightarrow \text{Case 1 : } \Gamma = 50\%$$

$$\text{Case 2 : } \Gamma = 37.5\%$$

$$T(\text{tors})\pm = 12.4\%$$

$$T(\text{flex})\pm = 25.1\%$$

Optimise for case 2:

$$a_s = 70 \mu\text{m} \text{ and } a_t = 41 \mu\text{m} \rightarrow \text{Case 1 : } T = 37\%$$

$$\text{Case 2 : } T = 50\%$$

$$T(\text{tors}) \pm = 16.5\%$$

$$T(\text{flex}) \pm = 33.5\%$$

Practical dimensions:

$$a_s = 100 \mu\text{m} \text{ and } a_t = 100 \mu\text{m} \rightarrow \text{Case 1 : } T = 40.2\%$$

$$\text{Case 2 : } T = 34\%$$

$$T(\text{tors}) \pm = 11.2\%$$

$$T(\text{flex}) \pm = 22.8\%$$

4.3.5 Possible improvements.

The 'side-fibre' torsional wave birefringent fibre frequency shifter has been demonstrated although at low efficiency. This shifter design is both novel and desirable due to its use of a readily obtainable fibre and the convenient 3 MHz shift frequency. Future work could concentrate on improving the efficiency and ruggedness of this design along the lines suggested in section 4.3.4.

A second version of this shifter incorporated a generator which requires only one joint to be made during manufacture. This is achieved by making a 90° bend at the tip of the silica spike during manufacture (see fig 4-6), ensuring that $a_t = a_s$ (in the above calculations this gives 82% coupling from the tip to the side fibre), and removing the possibility of a 'bad' joint, thus making the system more rugged. However, the bends produced so far are fairly gradual and do not give as efficient conversion of the longitudinal wave to the flexural wave as hoped. Another advantage is that the length of the 'side fibre' formed by the spike tip may be pre-cleaved to an exact (small) number of half-flexural-wavelengths prior to jointing. This should optimise coupling to the torsional wave on the main fibre rather than to the flexural wave. This is also possible for a separate side fibre design, though longer lengths may have to be used.

Torsional acoustic wave fibre frequency shifters based on the side-fibre and 90° bend spike configuration torsional transducers were demonstrated, giving a frequency shift of 3.2MHz and a maximum conversion efficiency of 6%. It was thought that, although a large degree of optimisation of the acoustic design was still possible, alternative designs of torsional transducer should be investigated to give a far more rugged device.

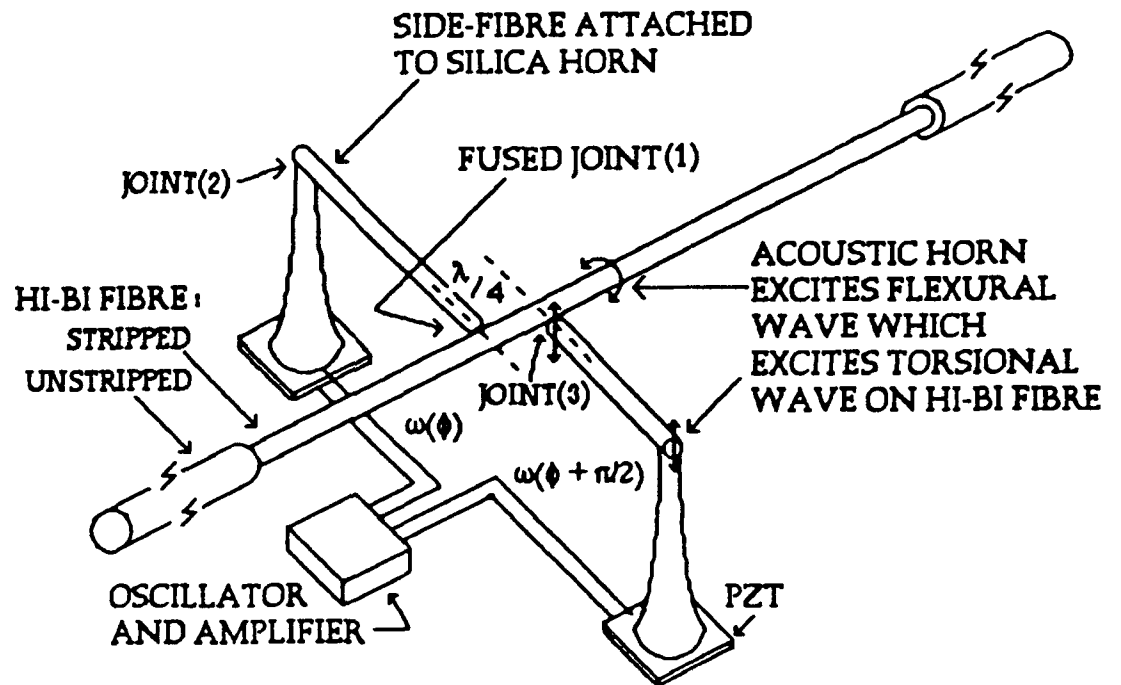


Figure 4-1 : Torsional wave generator configuration

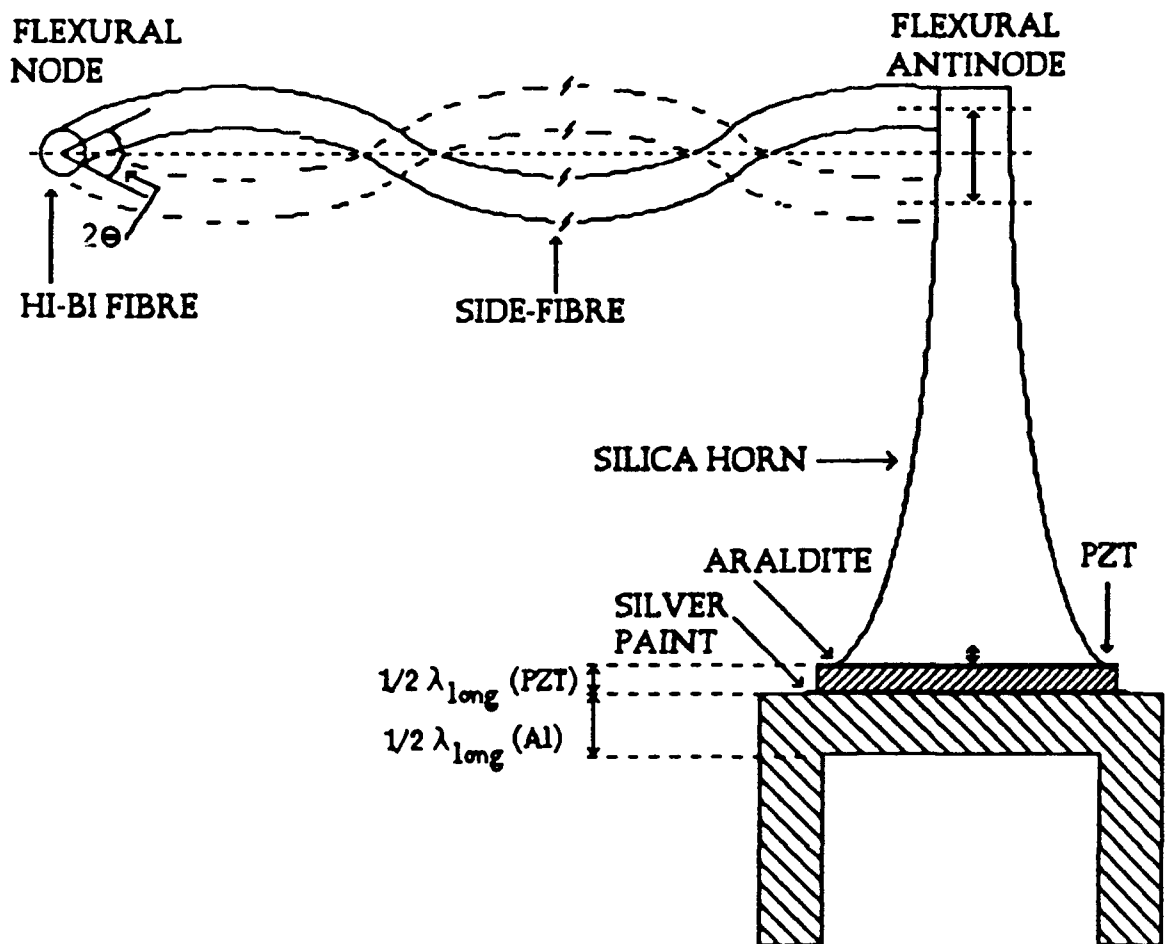


Figure 4-2: Schematic of torsional wave generation

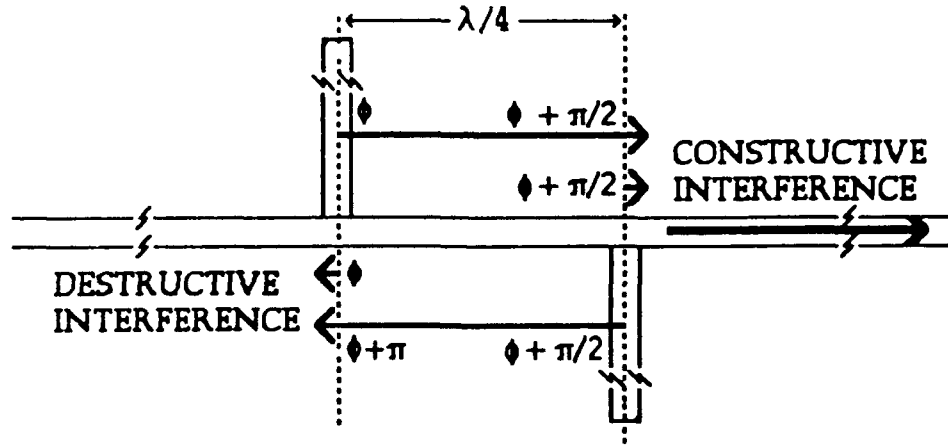


Figure 4-3 : Cancellation of backward propagating wave

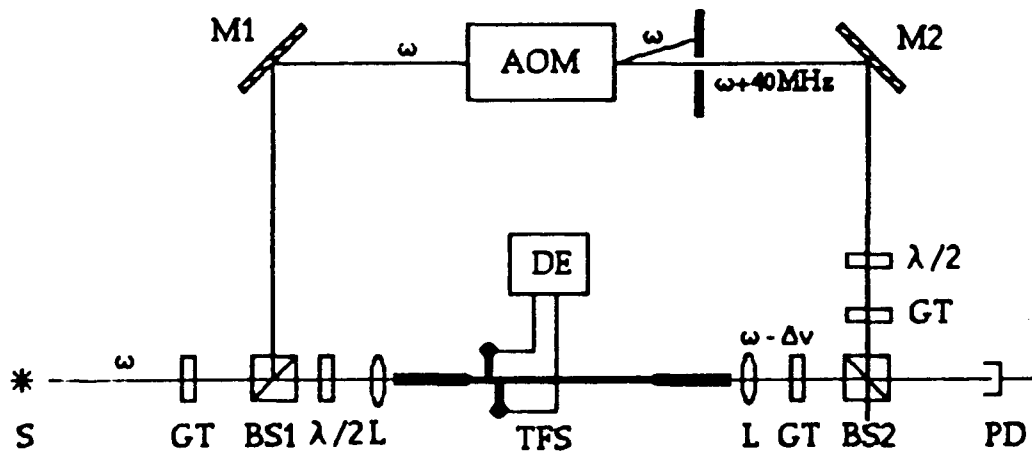
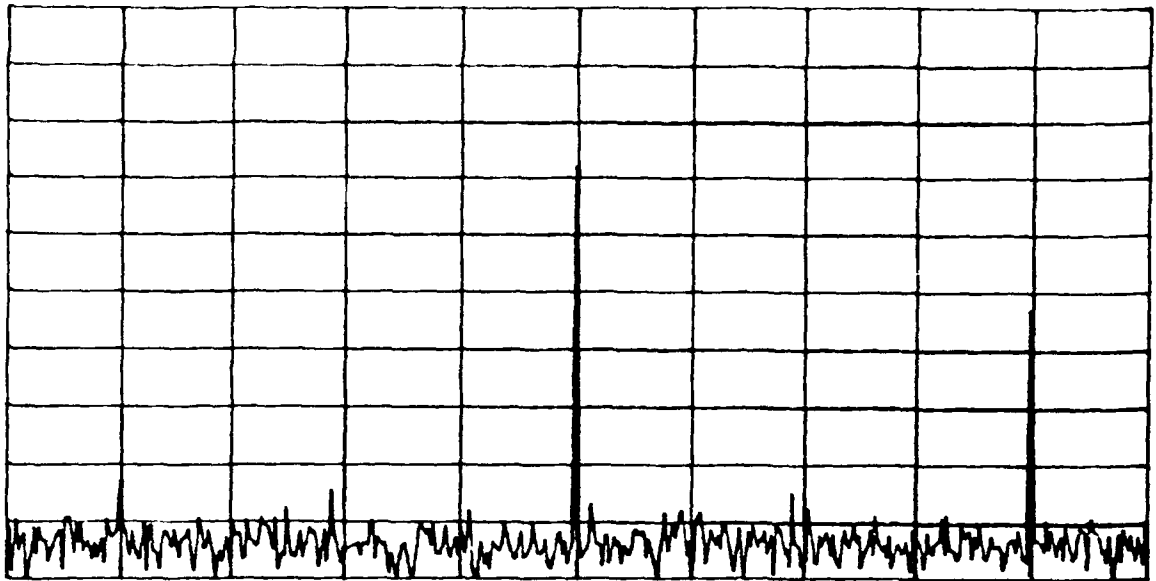
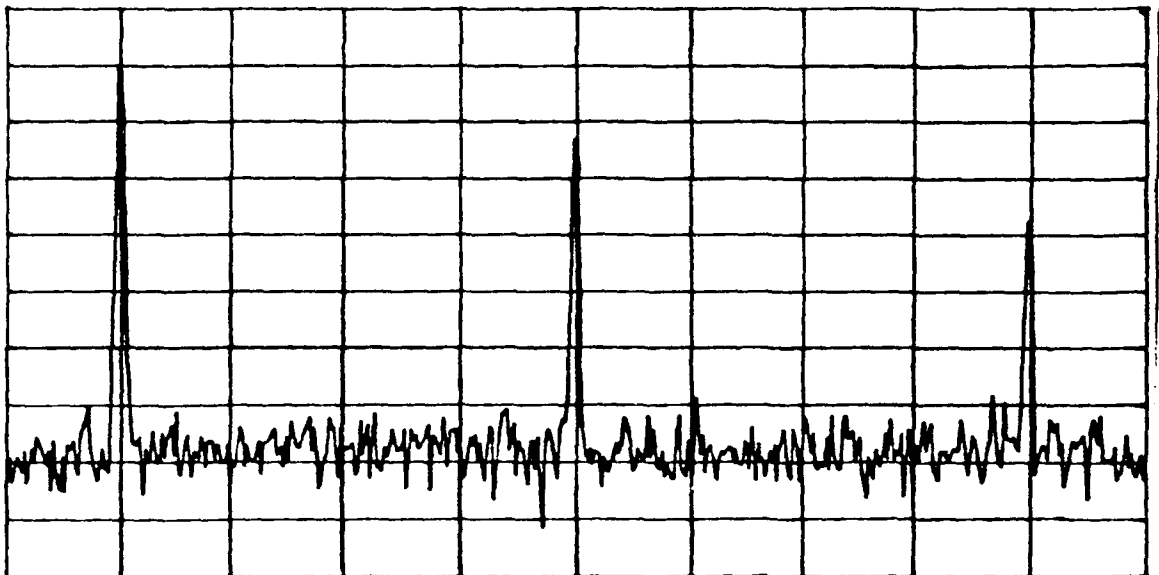


Figure 4-4 : Shifter evaluation configuration

S: optical source, GT : Glan-Thomson prism polariser, BS1/2 : beamsplitters, L : lens, $\lambda/2$: halfwave plate, TFS : torsional wave fibre frequency shifter, DE : drive electronics, M1,2 : mirrors, AOM : acousto-optic modulator (Bragg cell), PD : detector



(a)



(b)

Figure 4-5 : Spectra obtained by coupling from
 (a) fast→slow axis = upshift ; (b) slow→fast axis = downshift
 in each case the drive frequency was 3.195MHz.
 Vertical scales: Amplitude ; 5dB/div; Upper limit = -50dBm
 Horizontal scales: Frequency; 800 Hz/div; Center = 40MHz

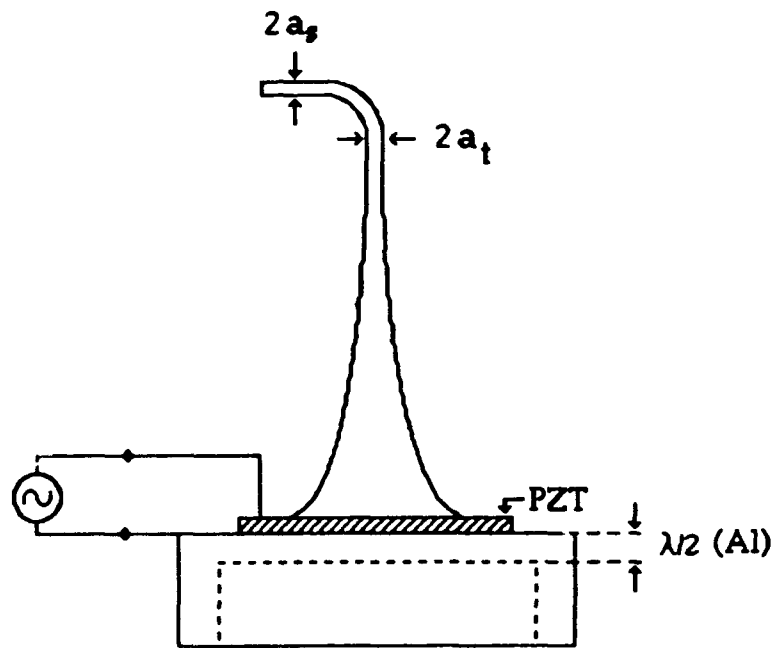


Figure 4-6 : Schematic of silica spike incorporating 90° Bend

4.4 Torsional acoustic wave hibi fibre frequency shifter II : 'In-line' configuration.

4.4.1 Introduction.

A far more rugged torsional transducer design was conceived in the form of an in-line acoustic horn with an axial capillary bore through which the birefringent fibre could pass and be joined to the horn tip. A torsional wave excited at the large diameter end of the horn would then be amplified within the acoustic horn and transmitted onto the optical fibre (see diagram 4-7).

The operation of the tapered silica horn as an amplifier can be readily understood from the conservation of energy in a rotating system where the rotating object has a decreasing moment of inertia, as it is clear that an increase in rotational amplitude, proportional to the ratio of the initial and final diameters, should occur. This will be the case so long as the change is smooth and gradual. Excitation and coupling between higher order torsional modes may occur but it is difficult to envisage coupling to any other types of acoustic modes (longitudinal, flexural, radial). Hence, the ideal acoustic horn has a large base to tip diameter ratio, and a precision coaxial bore with a diameter equal to that of the fibre. In addition, to maximise the efficiency of transfer of acoustic power from the horn to the fibre, the horn tip diameter should be very similar to that of the fibre, and they must have similar acoustic properties. Hence, the velocity of sound in the horn material must be well matched to that in silica, and for optimum performance the horn must be constructed from silica.

As the efficiency of the transducer depends critically on the surface finish of the cone and the concentricity of the bore, we approached several precision glass fabricators to ascertain if prototype units could be manufactured. Unfortunately we were not able to find a manufacturer who was prepared to undertake the work. It was therefore necessary that we attempt to modify existing optical components or fabricate the horn ourselves. The techniques developed to fabricate the acoustic horns are presented in section 4.4.3.

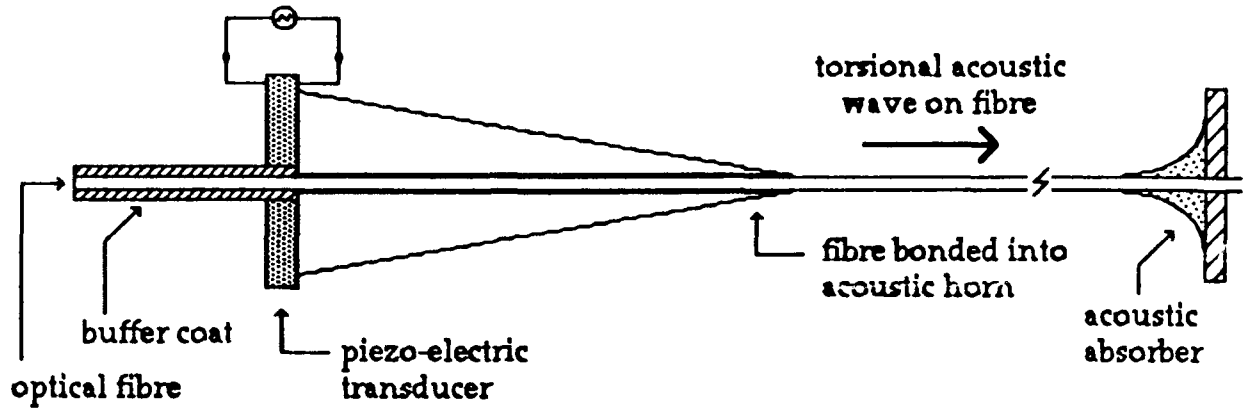


Diagram 4-7: In-line acoustic horn shifter schematic.

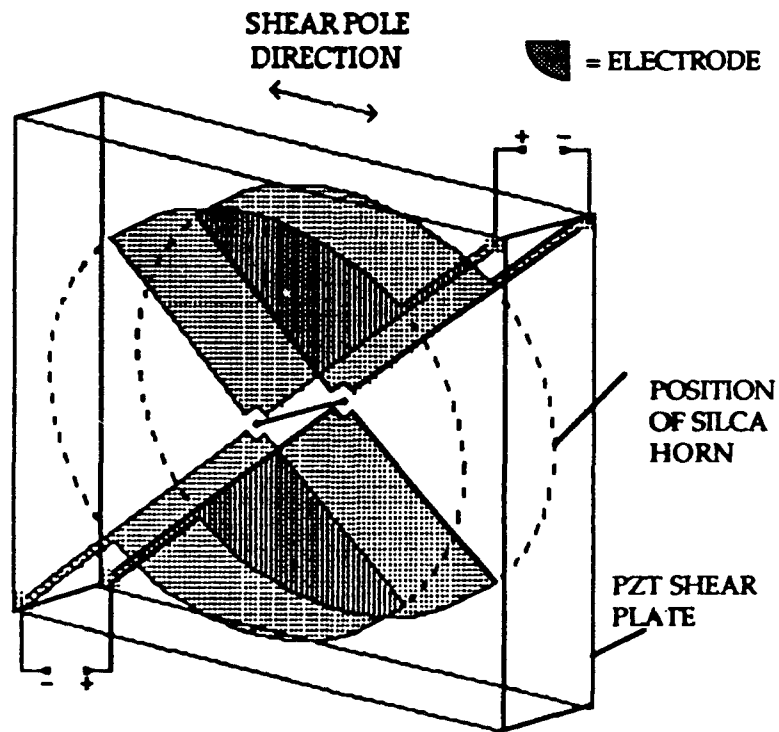


Diagram 4-8: Shear plate torsional transducer (type A).

A literature search was carried out to review work on the excitation of torsional acoustic waves, particularly on rod-like structures. The literature contained several examples of work carried out on torsional acoustic delay lines. Unfortunately, none of these methods for generating torsional acoustic waves were applicable to the optical fibre frequency shifter. However, one piece of work [16], on acoustic waveguides, used a torsional acoustic wave generator which appeared to be directly applicable to the excitation of torsional waves on an acoustic horn. This and other methods of fabrication of torsional acoustic wave generators are discussed in section 4.4.2.

4.4.2 Fabrication of piezo-electric torsional generators.

4.4.2.1 Bow-tie design.

The first design of torsional transducer investigated, which could be attached to the acoustic horn, was similar to that used by Boyd et al [16] and is designated type A. Figure 4-8 shows a schematic of this design, which consisted of an appropriately poled piezo-electric shear plate, onto which a layer of aluminium was deposited and then a 'bow-tie' pattern of electrodes was lithographically etched. In order to induce torsional shear motion, the two halves of the piezo-electric transducer are driven in antiphase.

The piezo-electric shear plate (Vernitron PZT-7A) had a resonance frequency of ~3 MHz, so as to generate torsional acoustic waves with a wavelength matched to the beatlength of the birefringent fibre. The 3MHz PZT transducer was ~0.6mm thick, and as the material is rather brittle, the unmounted shear plates are very fragile and must be handled with extreme care.

Techniques were devised for cutting the piezo-electric plates to size with a diamond impregnated saw, drilling the central hole for the optical fibre and lithographically etching the electrode pattern onto each side, having previously deposited aluminium.

In order to confirm the operation of these shear plates prior to final construction of the torsional device it is necessary to probe the torsional

amplitude at the shear plate surface. The method of evaluation is described in section 4.4.4.2.

Alternative implementations for the torsional acoustic wave transducer, requiring far simpler fabrication, are shown in the diagrams below. Figure 4-9 (type B) and 4-10 (type C) show two designs for coupling shear plates to tapered horns.

4.4.2.2 Side shear plate design.

The design of the torsional acoustic wave generator shown in figure 4-9 (type B), is based upon exciting antiphase shears at points of contact at the ends of a diameter of the acoustic horn cross-section. This design was implemented by bonding two piezo-electric shear plates to the horn as shown in figure 4-9. The shear plates were then electrically excited in antiphase.

This design is limited in its application for two reasons (i) it suffers from the fragility of the line contact between the piezo-electric transducer and acoustic horn, and (ii) the stress field produced by the shear plates is also a relatively poor match to the fundamental torsional mode in the horn, as it is a linear function of radius.

The spectrum of the torsional vibration excited on a solid silica acoustic horn with a type B torsional generator is discussed in section 4.4.5.1.

4.4.2.3 Base mounted PZT shear plates.

A third type of piezo-electric shear plate based torsional acoustic wave generator, type C, was fabricated, and is shown schematically in figure 4-10. This design is more rugged and is based upon a number of triangular piezo-electric shear plates, positioned symmetrically around, and bonded to, the base of the acoustic horn (figure 4-10 shows the layout for a four element pzt drive unit). The poling and electrical excitation of the shear plates are arranged such that the generated shears all follow an approximately circular (clockwise, say) direction. The triangular shape gives a shear amplitude which increases from the centre of the horn to the edge. Hence, the combined stress fields provide a better approximation to

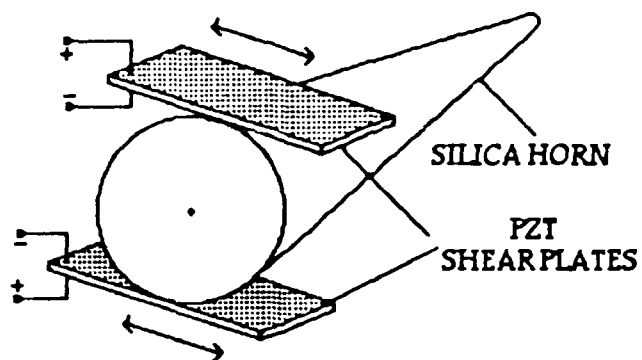


Figure 4-9 : Schematic of shear plate/silica horn transducer :
side attachment (type B).

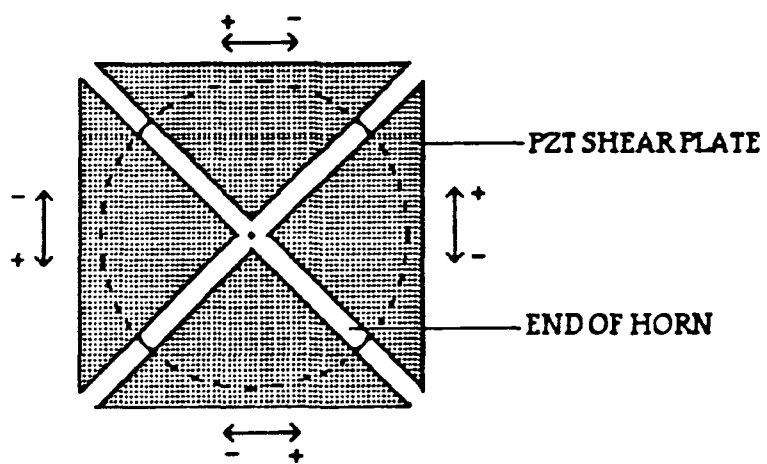


Figure 4-10. : Schematic of shear plate/silica horn transducer :
end attachment (type C).

the fundamental torsional mode (the larger the number of transducers, the better the approximation). Generators have been produced with four transducers bonded to both (i) solid, drawn silica horns and (ii) ground tapered Pyrex capillary tubes, and with six transducers bonded to a drawn Pyrex capillary tube. The performance of these devices is reported in section 4.4.5, and the methods of fabrication of the acoustic horns are discussed in section 4.4.3.

4.4.3 Fabrication of acoustic horns.

4.4.3.1 Introduction.

Several different techniques have been developed to fabricate acoustic horns which are a good approximation of the ideal design discussed in section 4.4.1. Figure 4-11 (type D) shows the ideal horn design, with a single fine bore. Figures 4-12 (type E) and 4-13 (type F) show alternatives that may also be acceptable, and are in principle easier to fabricate. The acoustic horns shown have a conical taper, however a gradual exponential taper is equally acceptable.

Solid silica acoustic horns have been fabricated by heating and drawing down silica rod on a glassblowers lathe. To produce an acoustic horn with a fine bore, one must either start with precision bore capillary tubing, rather than solid rod, or drill a bore through a solid horn. No suitable source of precision bore capillary tubing in silica could be found, however this was available in Pyrex. Pyrex has very similar acoustic properties to silica and is thus an acceptable substitute during prototype development. The outer diameter of the base of the acoustic horn governs the attainable amplification (for a given tip diameter). The smallest bore diameter available with reasonably thick walls was $\sim 250\mu\text{m}$, with an outer diameter of $\sim 6\text{mm}$. The methods for fabricating tapered capillaries having potential for the acoustic horn torsional generator are presented in the following sections (4.4.3.2-5).

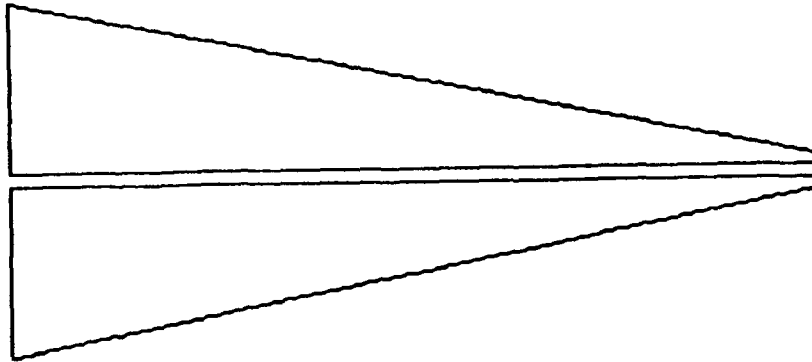


Figure 4-11 : Section through acoustic horn :
ideal case, single bore (type D).

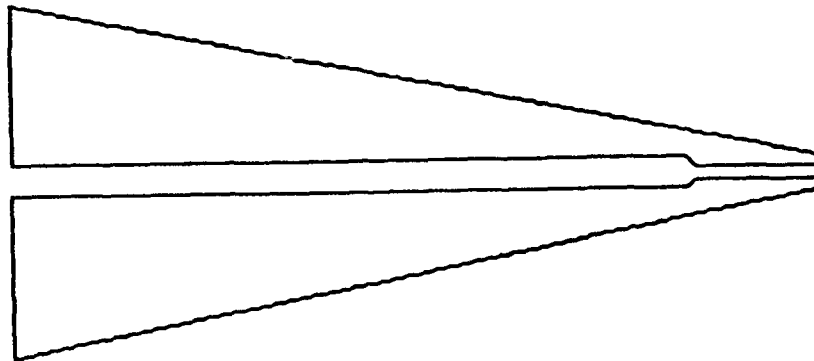


Figure 4-12 : Section through acoustic horn :
two bores (type E).

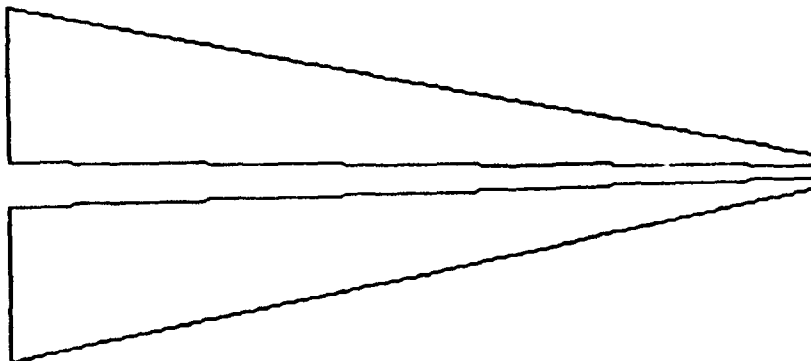


Figure 4-13 : Section through acoustic horn :
smooth bore transition (type F).

4.4.3.2 Pyrex capillary drawn onto tungsten wire.

The University glassblower attempted, unsuccessfully, to draw down capillary with a bore diameter equal to that of the jacketed fibre (~250 μ m) while heating it with a 150 μ m diameter tungsten wire supporting the inner bore. The problems encountered with this method were (i) the glass bonds to the metal wire, removal of the wire is difficult as either etching (with acid) or spark erosion must be used, and (ii) the wire tends to bend upon heating and the softened glass follows its shape. As it is necessary that the capillary bore is on axis at the tip of the horn, the wire must be kept under tension throughout the drawing process, which could not be easily achieved with the equipment available to us.

4.4.3.3 Ground tapered Pyrex capillary.

Prototype horns were manufactured for us by Jencons (Scientific) Ltd., (a supplier of precision bore capillary), by grinding the tube to form the taper. We also had tapered capillaries prepared, in a similar fashion, by the University glassblower.

The tapered capillaries had a bore diameter of ~250 μ m. The ground finish of the horn was fairly rough, but this could be improved by polishing. The performance of torsional transducers incorporating this form of tapered acoustic horn is presented in section 4.4.5.3.

The major problem encountered with this method of fabrication is that the concentricity of the bore varies along the length of the tubing. The grinding process produces a taper with an axis concentric with the outer diameter of the tubing. Consequently, the bore generally emerges off-centre at the horn tip. Concentricity of the capillary bore with the surface of the capillary is generally not required, hence the manufacturers do not control the capillary centration with high precision. This is highly undesirable in the torsional frequency shifter application, because as shown in figure 4-14, the vibration transmitted to the optical fibre, bonded at the horn tip, is torsional if the fibre is central, but increasingly flexural if the fibre is non-central.

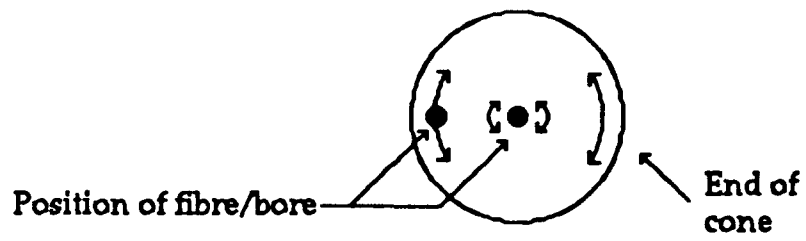


Figure 4-14 : Transmission of torsional or flexural waves depending on position of fibre in horn tip.

4.4.3.4 Drilling.

A tapered capillary acoustic horn (type D) may be fabricated by drilling the bore through a solid horn. We consulted various companies involved with drilling fine holes by different techniques (conventional drilling, laser drilling, ultrasonic drilling, etc.). These techniques may be applied to drill a fine bore hole (150 - 300 μ m diameter) but are limited to a drilling depth of a few millimeters. In glass, the problems of drilling are worse than in most metals and so we considered using a metal cone. Aluminium has a shear wave velocity closer to that of fused quartz than most metals, and its low density gives a torsional acoustic impedance very close to that for fused quartz, hence it appears to be an acceptable substitute material for the horn. Furthermore, being conductive, a drilling technique called electro-discharge machining (EDM) may be used. With this technique bore diameters as small as 300 μ m can be drilled to a depth of a few cms.

Figure 4-12 shows a cone with two concentric bores (type E). Both bores are drilled conventionally, the finer bore (approx. 250-300 μ m) is drilled as centrally as possible from the horn tip to its maximum depth (a few mms), then the larger bore is drilled from the large O.D. end to meet the fine bore. Type (E) may be produced, by conventional drilling of aluminium, in our laboratory workshops, though the bore discontinuity may give rise to acoustic mode coupling. Figure 4-13 shows a cone with a gradually decreasing bore diameter as well as outer diameter (type F). Type F horns should be produced by the EDM technique.

We are in contact with the University of Birmingham (U.K.) who have recently acquired an EDM machine, and they have agreed to try to drill fine bores in the acoustic horns as soon as their machine is operational. Meanwhile, we have experimented with aluminium cones to demonstrate that we can excite torsional acoustic waves in the same manner as for silica horns, and to find the best way to join the fibre to the aluminium horn tip (either by soldering a pre-metallised fibre or by the use of an adhesive), this work is at present incomplete.

4.4.3.5 Drawn Pyrex capillary acoustic horn (type F).

Production of a type (F) device has been tried by both the university glassblower (on a glassblowers lathe) and in our laboratory (with motorised translation stages and an oxy-propane torch). We have used 8mm O.D. Pyrex capillary with a 1mm bore, which can be drawn down to an O.D. of <1mm to give a bore of <200 μ m. Difficulties encountered are in preventing the bore closing entirely and, again, achieving a concentric bore at the tip.

The university glassblower has however managed to produce several drawn capillary acoustic horns (type F) suitable for use in an in-line configuration fibre frequency shifter. The method of fabrication and performance of this device are reported in this section and in section 4.4.5.4, respectively.

The drawn capillary acoustic horns were made from pyrex capillary tubing with an initial outer diameter of 7.9mm and a bore diameter of 1mm. The Pyrex tubing had very good bore concentricity. Drawing this tubing down on a glassblowers lathe (plus initially expanding the bore using gas pressure) has enabled us to fabricate a horn with a bore as small as 40 μ m with a tip outer diameter of 350 μ m, over a length of approximately 40mm. Cleaving the horn tip back to a point where the bore is 125-130 μ m (the fibre diameter) gives a tip outer diameter between 0.6 and 1mm; giving an outer diameter ratio in the range 1:9 to 1:14. The bore centrality at the horn tip is excellent.

4.4.4 Measurement of torsional vibrations.

4.4.4.1 Introduction.

Torsional vibrations of a bulk object can be studied using a modified Doppler difference anemometer, and two rather expensive systems are available commercially. Apart from the expense, these devices are not ideally suited for the measurements required to assess the performance of the frequency shifter, and we have designed, but not yet implemented, a fibre optic based torsional vibrometer. Torsional vibrometers are normally used to analyse the performance of rotating shafts, as the measurement is independent of shaft profile and translational motion. A shaft rotating at constant angular frequency gives a constant Doppler difference frequency directly related to the shaft's angular velocity. In our case the angular velocity is changing at the rate defined by the sinusoidal excitation and hence its spectrum will be more complex.

4.4.4.2 Evaluation of type A torsional transducer.

A conventional bulk-optic laser Doppler velocimeter was constructed in order to measure the surface displacement of the shear plate in a type A torsional transducer. The velocimeter was tested by measuring the surface velocity of a rotating glass disc. When used to observe the surface rotation of the shear plate transducer, no frequency shift was detected. It was thought that the lack of observed shear plate motion could have indicated that the shear plates were being damaged during the lithographic process and subsequent mounting. Prior to this processing, a conventional heterodyne linear vibrometer (as shown in figure 3-4) had been used to measure the vibration of the shear plate edge. In this measurement the piezo-electric transducer was electrically excited using the original unfired silver-paint electrodes supplied by the manufacturer. This silver paint is unsuitable for lithography and must be removed and replaced with a thin layer of aluminium, in order to produce the desired electrode pattern. Post-lithography measurement of vibration by this technique was not possible due to the inaccessibility of the moving (electroded) surface.

Due to the complexity of the lithographic process and the lack of observable motion, type B and C transducers were fabricated in preference to type A.

4.4.4.3 Measurement of vibration along the acoustic horn.

As the vibrational amplitude produced by the shear plates is small, the torsional transducers were coupled to acoustic horns in order to amplify the vibration prior to measurement. The torsional vibration amplitude could then be probed at the surface of the horn. The ideal device for the measurement of torsional vibration amplitude would be the optical fibre based torsional vibrometer discussed above. This device is not yet available and bulk-optic velocimeters are impractical given the small size of the horn.

A new technique was developed in order to observe the vibration of the horn, which required the attachment of small reflectors (short sections of tinned wire) to its side. The heterodyne linear vibrometer was then arranged to measure the translational motion of these reflectors, at the edges of the horn, and also at the centre. The combination of these measurements indicates the relative amplitudes of translational (flexural and radial) and torsional vibration of the horn.

4.4.5 Results of torsional measurements.

4.4.5.1 Type B transducer with solid silica horn.

A type B transducer was constructed, from a solid silica rod drawn into a taper (outer diameter: 4mm-0.4mm) and two piezoelectric shear plates (10mm x 5mm). The vibration of this horn was measured, using the technique described in section 4.4.4.3, and found to be mainly torsional, with a maximum tip amplitude of ~15nm, see figure 4-15. Measurements taken at different positions on the horn indicated an amplification factor proportional to the ratio of outer diameters, as expected.

4.4.5.2 Type C transducer with solid silica horn.

A type C torsional transducer, consisting of four piezo-electric shear plates arranged as in figure 4-10, was bonded to a solid horn with a larger outer diameter of 10mm and tip diameter ~0.5mm. The vibration was tested as before. Again, predominantly torsional vibration was observed, as shown by the spectra of figure 4-16. Figure 4-16(A) shows the maximum vibration (peak amplitude approx. 400nm) measured at the edge of the horn tip corresponding to the total torsional and translational motion, whereas figure 4-16(B) shows the vibration (peak amplitude approx. 15nm) measured at the centre of the tip with the same drive voltage. For a perfect torsional transducer the angular velocity at the axis should be zero, hence the signal observed from the centre of the tip can be assumed to be caused by translational motion. If the torsional vibrometer were available it would be possible to determine the torsional motion uniquely. This residual translational motion may be attributed to asymmetries in the positioning of transducers, the shape of the horn and the perturbation due to the attachment of the reflectors. The drive voltage to this device was increased while the vibration of the edge of the tip was measured, and the values for which the J_0 and J_1 components were minima were noted. At these points, the vibration amplitude can be calculated absolutely. The graph of drive voltage versus peak vibration amplitude, figure 4-17, was

plotted using these values. Figure 4-18 shows the spectrum when the drive level corresponds to the first minimum of J_1 , here the amplitude is $\sim 193\text{nm}$ (optical wavelength of vibrometer source = 632.8nm).

4.4.5.3 Type C transducer with ground tapered Pyrex capillary horn.

Type C transducers (four pzts) were also bonded to ground capillary horns with a maximum O.D. of 5mm and a minimum O.D. of $\sim 1.6\text{mm}$, giving a diameter ratio (3.1), smaller than that of the previous device. The maximum tip amplitude measured with this device was approximately 15nm , figure 4-19. This is the largest O.D. capillary we have been able to locate with a bore approaching the fibre O.D. (bore diameter = $250\mu\text{m}$). Unfortunately, the bore of this capillary was not concentric with the O.D. and hence, when the O.D. is ground to give a taper, the bore emerged off-centre at the smaller O.D. end. As discussed in section 4.4.3.3, an off-centre capillary will transmit flexural rather than torsional acoustic waves. This was confirmed when a stripped highly birefringent fibre was placed through the horn capillary and attached to the tip. This device was evaluated in the heterodyne interferometer (figure 4-4) so that the relative amplitudes of the torsional and flexural waves, excited on the fibre could be measured, as with previous fibre frequency shifters. No frequency shifting, at the torsional wave frequency, was observed. When the tip vibration was measured 'in situ' it was found to be only slightly less than before the fibre was introduced. The vibrometer was then focussed on the fibre itself, close to the tip. A small flexural amplitude was observed (of the order of $5\text{-}10\text{nm}$). Consequently, we can conclude that the only significant acoustic wave excited on the optical fibre was a flexural wave.

Close inspection of the commercially supplied ground capillary horns indicated that similar results would be achieved, hence other possible methods for producing the horns were considered necessary.

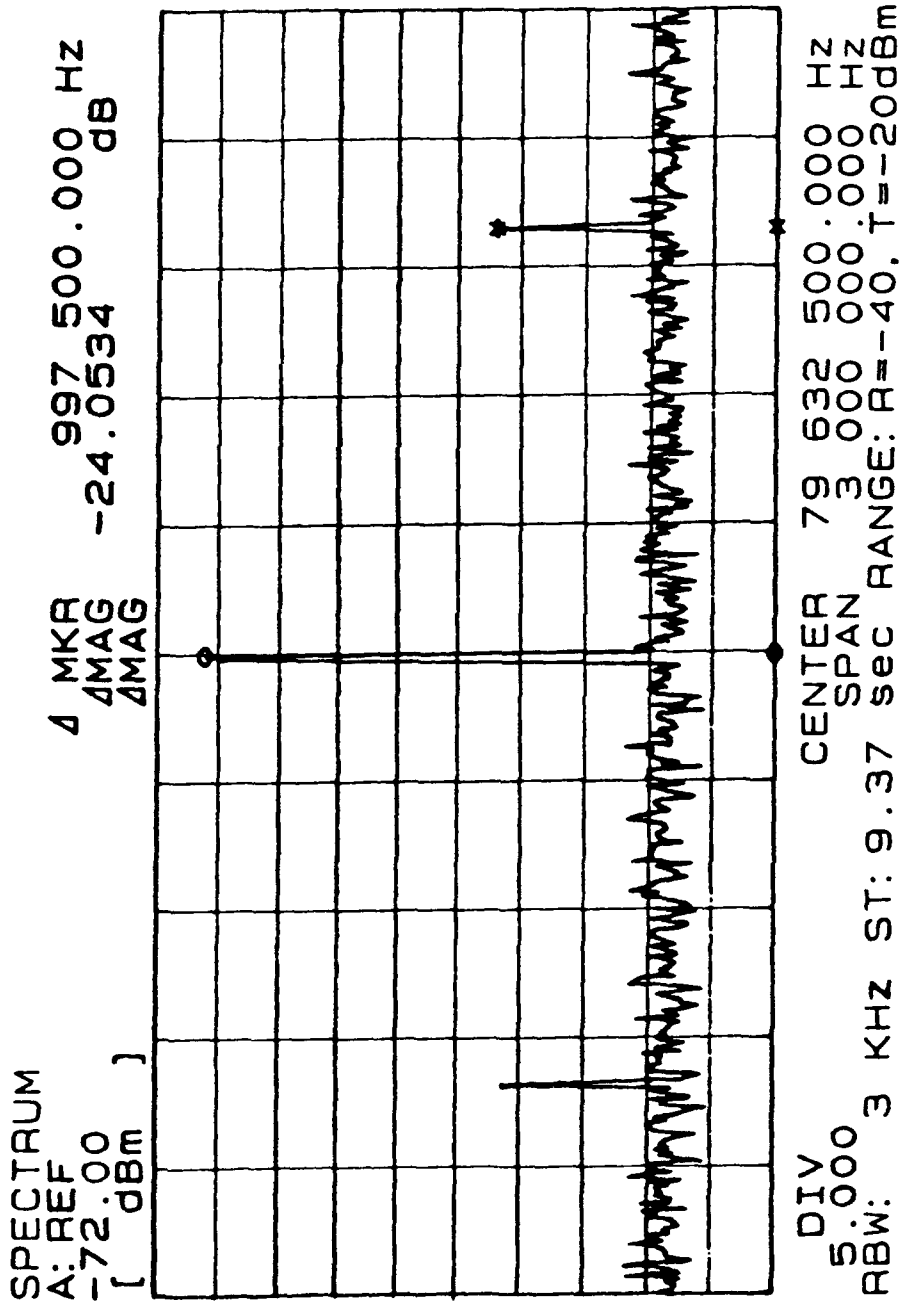


Figure 4-15 : Heterodyne vibrometer output spectrum : Edge of tip of type (B) transducer with solid, drawn silica horn (diameter ratio 10) . Carrier frequency = 40MHz, pzt drive frequency = 1MHz, pzt drive voltage = 30V.

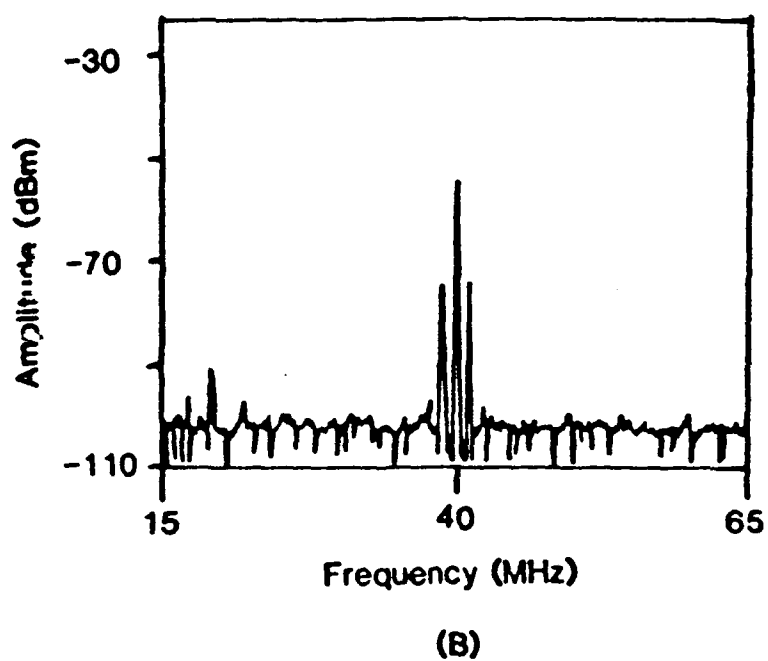
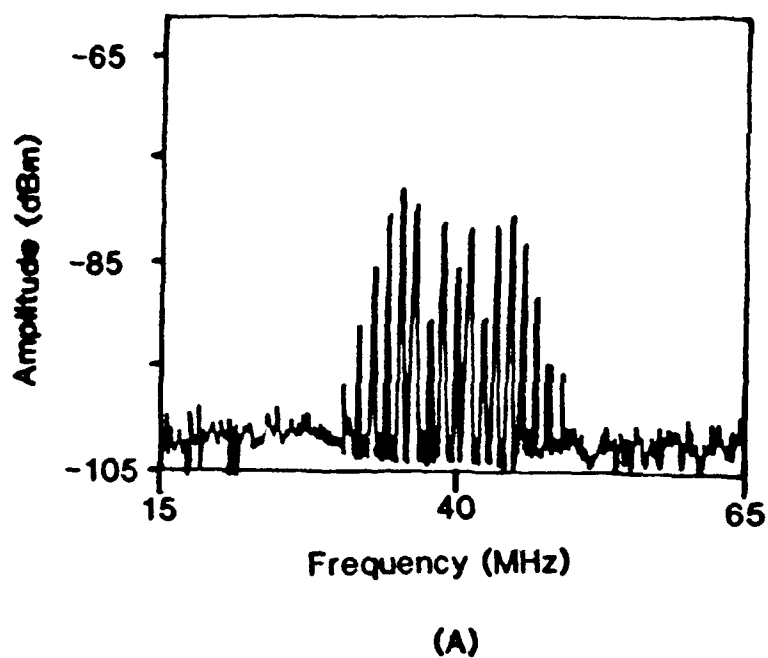


Figure 4-16 : Heterodyne vibrometer output spectrum : Edge of tip of type (C) transducer with solid, drawn silica horn (diameter ratio 20) . Carrier frequency = 40MHz, pzt drive frequency = 1.24MHz, pzt drive voltage = 12.5V:
 (A) Edge of tip (B) Centre of tip.

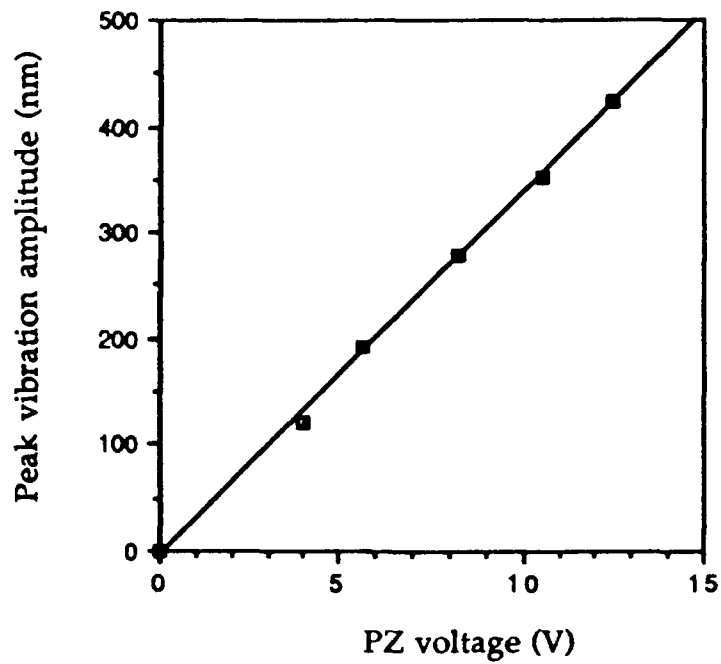


Figure 4-17 : Graph of pzt drive voltage versus peak vibration amplitude.

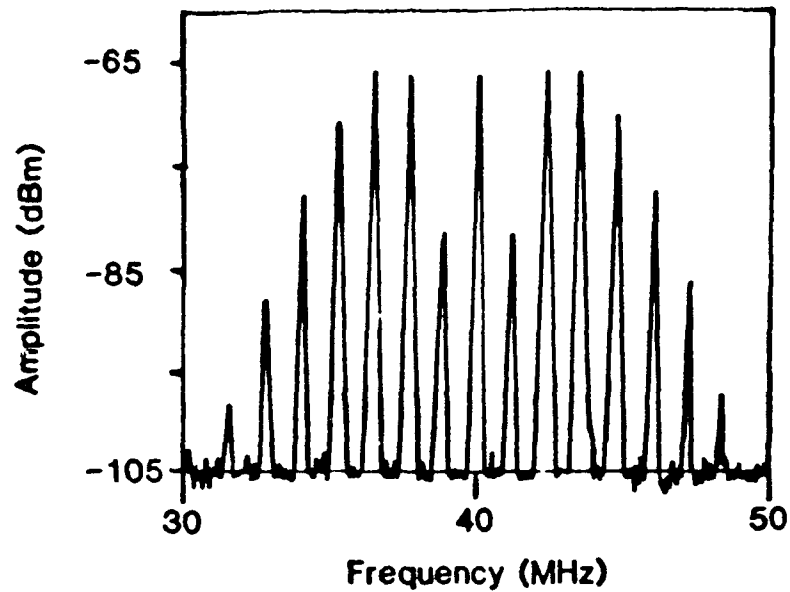


Figure 4-18 : Heterodyne vibrometer output spectrum : Edge of tip of type (C) transducer with solid, drawn silica horn (diameter ratio 20). Carrier frequency = 40MHz, pzt drive frequency = 1.24MHz, pzt drive voltage = 5.6V.

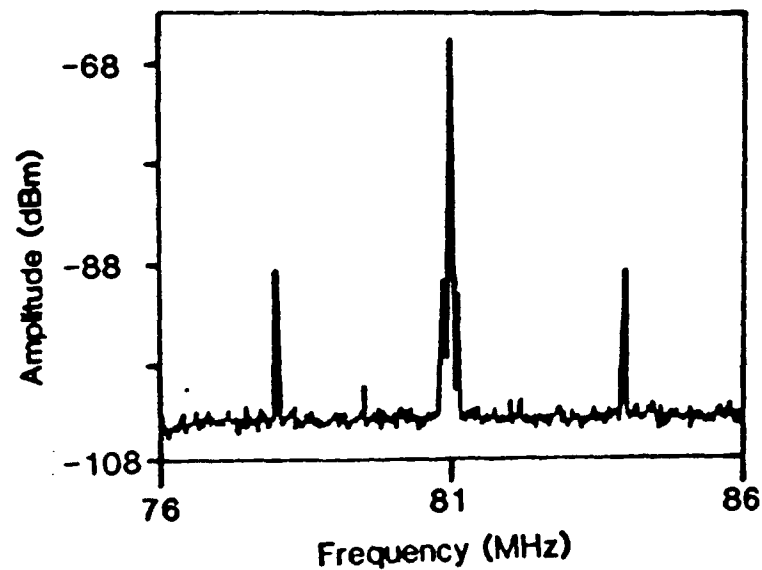


Figure 4-19 : Heterodyne vibrometer output spectrum : Edge of tip of type (C) transducer with ground capillary silica horn (diameter ratio 3.1) . Carrier frequency = 81MHz, pzt drive frequency = 3MHz, pzt drive voltage = 20V.

4.4.5.4 Type C transducer with type F drawn Pyrex capillary horn.

A type F acoustic horn was achieved by drawing down Pyrex precision bore capillary tubing as described in section 4.4.3.5. A torsional generator was fabricated from this acoustic horn by attaching three pairs of 3MHz piezo-electric shear plate transducers to the base of the horn such as to form a hexagonal pattern. The maximum O.D. of the horn was 7.9mm and the tip O.D. was 0.6mm, giving the generator a diameter ratio of ~13. The vibration of this horn was investigated using the heterodyne linear vibrometer as before with small reflectors attached near the tip. The vibration is again, as expected, predominantly torsional, although the vibration amplitude was less than expected, given the six transducers and diameter ratio, at approximately 10 to 15nm.

The bore concentricity of this acoustic horn was excellent, and hence it should transmit a torsional acoustic wave to an optical fibre bonded to the tip.

4.4.6 In-line torsional acoustic wave fibre frequency shifter.

4.4.6.1 Fabrication of in-line shifter.

Although the drive unit requires further development, it was decided to construct a fibre frequency shifter based upon the torsional transducer described in section 4.4.5.4, as this would establish if this approach for the frequency shifter was feasible. A highly birefringent fibre length was stripped and passed through the acoustic horn and supported at each end with silica rubber. The silica rubber acts as an acoustic absorber and defines the extremes of the acousto-optic interaction region. The fibre was then joined to the horn tip using silica jointing paste with the small oxy-propane gas torch. The gradually reducing bore allowed the fibre jacket to be left intact inside the horn right up to the point of the joint, although the heat from the torch caused this to burn back approximately 1cm. The fibre jacket should give good suppression of the unwanted sideband caused by any torsional wave propagating back from the horn tip, for example due to acoustic impedance mismatch at the joint. The fibre had an interaction length of approximately 46cm and was incorporated as one arm into a heterodyne Mach-Zehnder interferometer, as described in section 4.3.2, to investigate its use as a frequency shifter.

4.4.6.2 Results and discussion.

The shear plates were excited at a frequency of 3.2MHz and frequency shifting was observed immediately. The optimised drive frequency was 3.209MHz; consistent with the 3.195MHz optimum frequency obtained for the side-fibre torsional transducer shifter constructed previously. The low vibration amplitude gave rise to a maximum of only 2.5% optical power coupling efficiency, however sideband suppression up to 30dB was obtained. The carrier suppression was difficult to measure due to pick-up and breakthrough effects in the interferometer and detector, but we expect to achieve quite good suppression with the symmetry of the fibre to horn tip joint. Figures 4-20 and 4-21 show spectrum analyser traces of the detector spectrum with a

carrier (Bragg cell) frequency of 81.5MHz, drive frequency of 3.209MHz and drive voltage of 7.9V peak-to-peak. A different eigenmode is initially populated in each case, giving rise to the expected upshift and downshift for the different launching conditions. Figure 4-22 shows values of the optical power coupling efficiency, as measured on the spectrum analyser (in the same manner as in section 4.3.3), versus the applied drive voltage at a drive frequency of 3.209MHz.

Given a torsional amplitude of 10nm, an interaction length of 46cm and a fibre radius of 62.5 μ m, the theory for the torsional wave frequency shifter presented in section 4.2.2, gives a theoretical coupling efficiency of 14%. This is a factor of 5.6 times greater than the measured coupling efficiency of 2.5%. This is explained by the acoustic mismatch at the horn tip/fibre joint. With the present device the horn tip is ~5 times larger in diameter than the fibre. Hence, from the theory of section 4.3.5, the amplitude of the torsional oscillations on the fibre surface is ~5nm and hence the theoretical coupling efficiency is only 4%. The remaining discrepancy probably relates to an imperfect joint. We believe that higher efficiency devices may be constructed by improving the bonding between the piezo-electric shear plates and the acoustic horn, by further reducing the horn tip diameter to give an increased diameter ratio and by improving the horn tip/fibre joint.

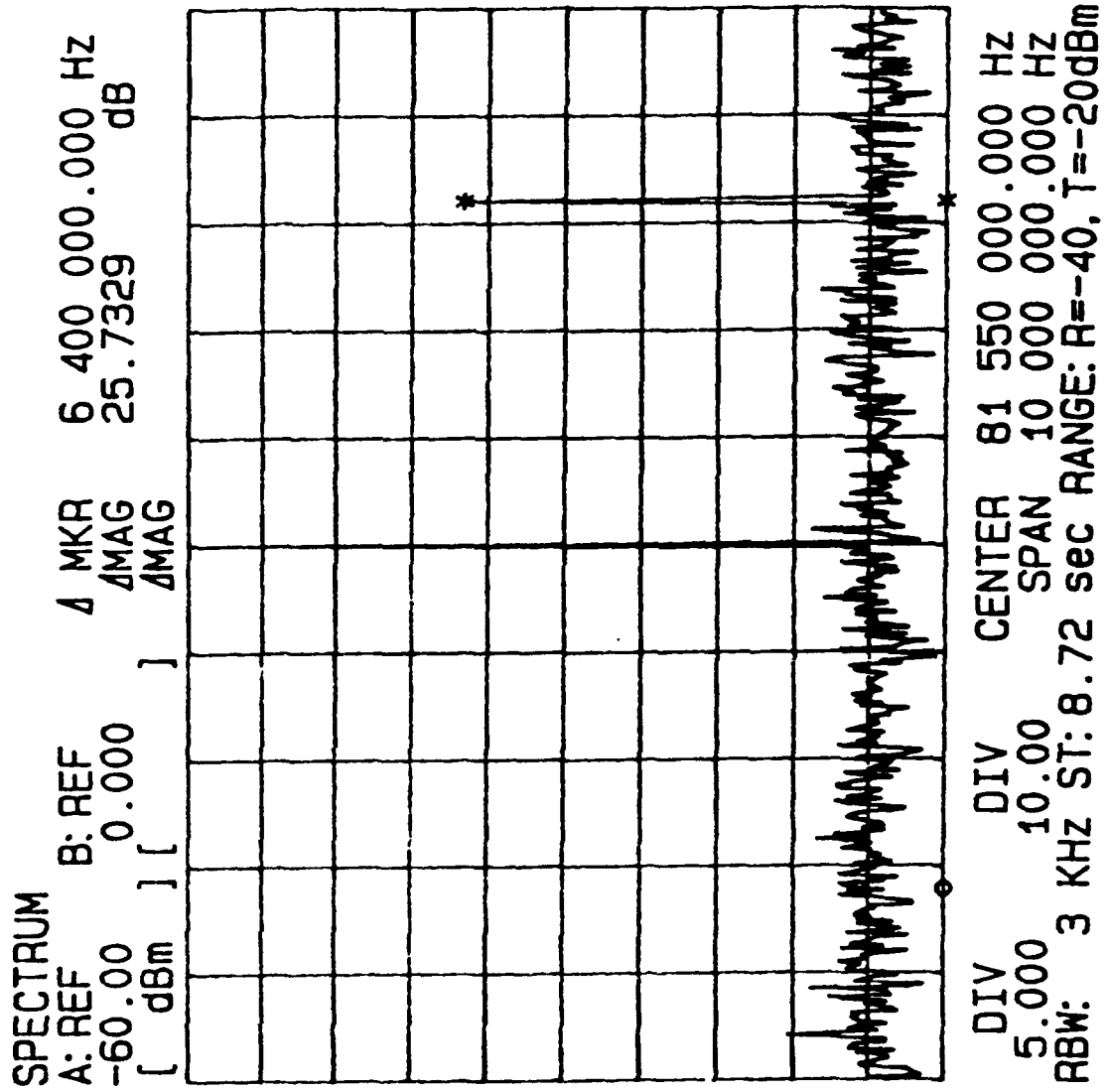


Figure 4-20

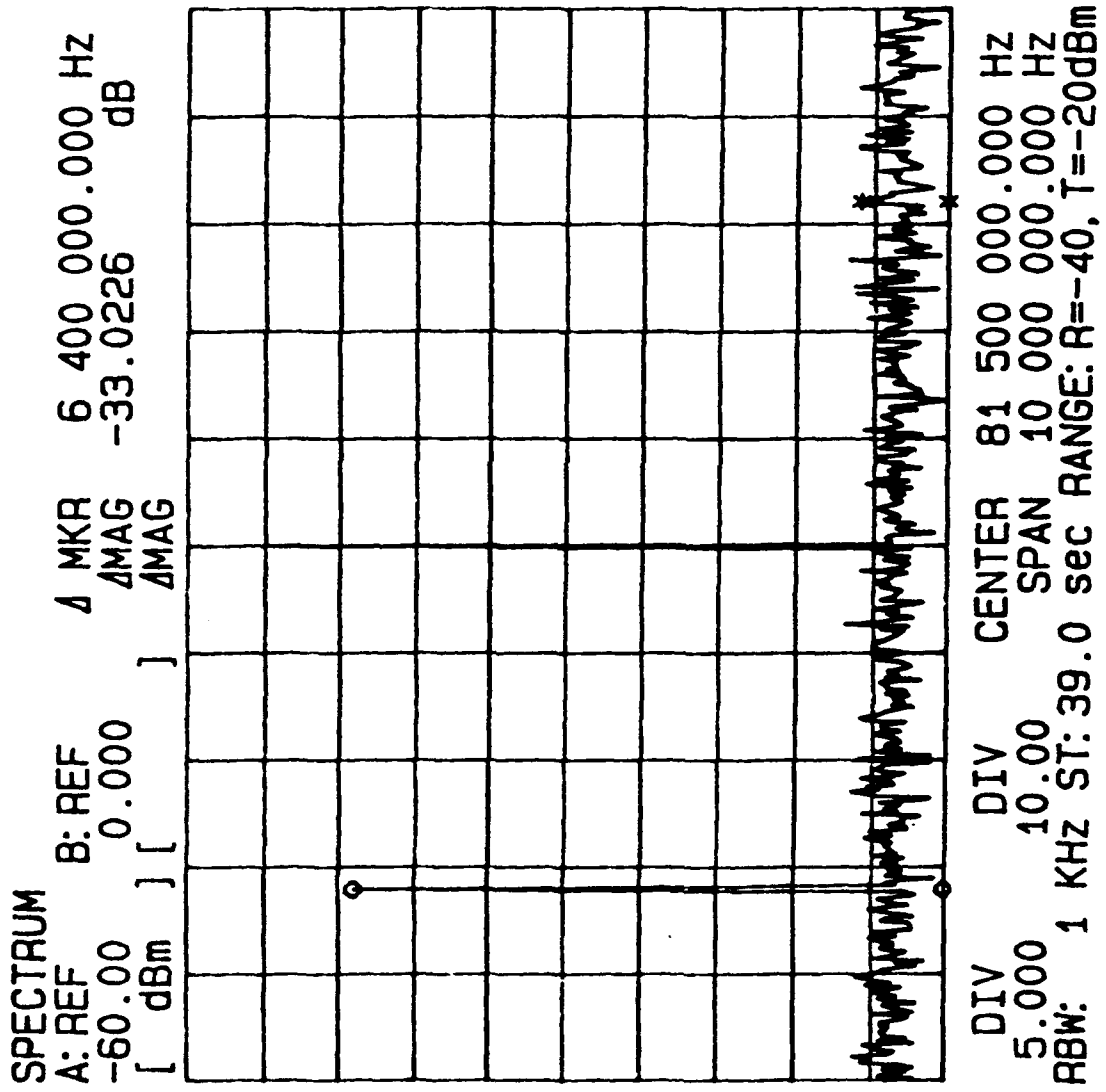


Figure 4-21

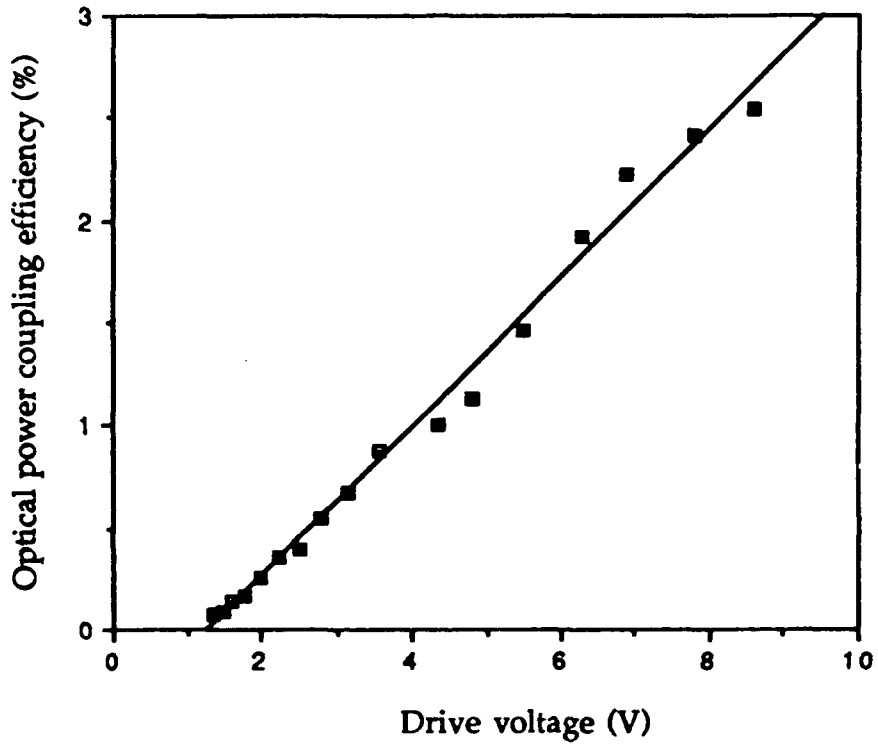


Figure 4-22 : Optical power coupling efficiency versus drive voltage.

5 Alternative frequency shifter configurations.

5.1 Surface acoustic wave device.

Several alternative mechanisms for producing a frequency shift in a fibre guided beam were considered and investigated at the same time as the birefringent devices described above. Surface wave devices have been developed by several workers in the field, but birefringent devices have not yielded high efficiency and have required very high electrical powers. The optical communications group working in the Electronics Laboratory at the University of Kent were investigating a device based on exciting surface acoustic waves on an planar active (piezo-electric) substrate with interdigital surface electrodes (see figure 5-1) [8].

It was proposed that as part of this project, a device using interdigital transduction of a surface acoustic wave on a piezo-electric cylinder, about which the optical fibre could be wrapped several times to increase the interaction length, might be feasible. Techniques were developed to prepare the piezo-electric cylinder surface, by polishing and vacuum deposition of a metallic (aluminium) layer while rotating the cylinder, and to photolithographically etch interdigital electrodes onto the surface. The electrode quality was severely impaired by the pitted surface of the sintered piezo-electric material available, making it virtually impossible to fabricate the fine electrodes required for a two moded fibre frequency shifter. Although a birefringent fibre shifter would require larger electrodes, the difficulty of production of high quality interdigital layers on this surface is equally great. The surface of the cylinder, even though polished, may also give rise to significant acoustic beam perturbation and spatial dispersion. Work on this form of shifter was discontinued while preferable shifter configurations were considered. The work carried out in the Electronics Laboratory, during a two year period, has not yielded a greatly improved shifter based on their planar substrate even with a double pass of optical fibre, which improves the efficiency provided that the phase relation between the first and second passes can be maintained constant. In practice this has proved difficult.

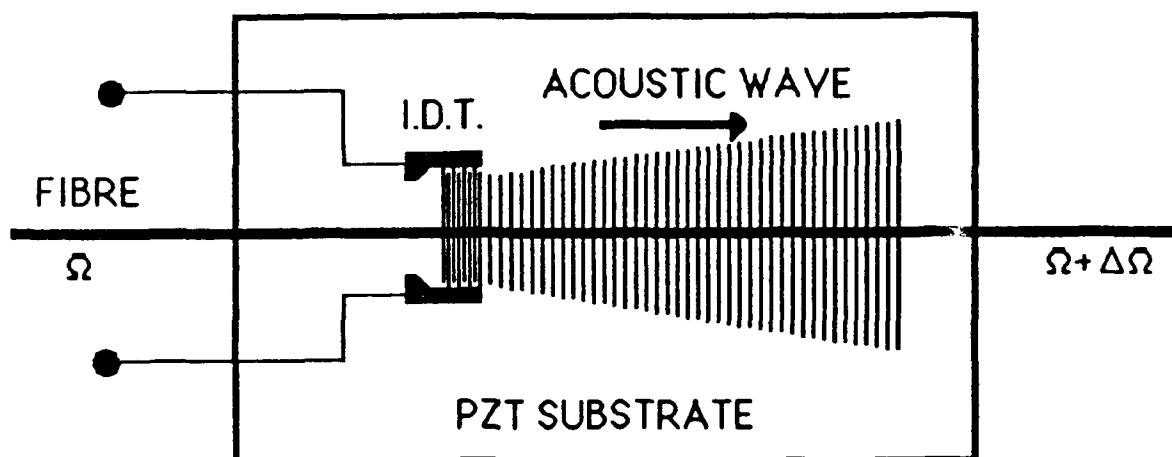


Figure 5-1: Interdigital transducer (IDT) based shifter.

5.2 Stimulated Brillouin scattering.

Alternative systems which could be born in mind as a source of frequency shifted light may be based upon the mechanism of stimulated Brillouin scattering (SBS). In optical fibres SBS is a relatively efficient process, with optical efficiencies of up to 50%. The SBS frequency shift in a typical optical fibre depends on the wavelength of the source and is typically between 10 - 30GHz i.e. in the microwave region. This frequency is clearly too high for general purpose signal processing, as this is generally carried out at 1 - 50MHz. It has been shown however that MHz signals can be generated by mixing two SBS signals produced in different fibres [17]. As SBS is a non-linear phenomenon, it does not occur until the input power is above a certain threshold power. In long lengths of the fibre this may be several milliwatts, however in low loss ring resonators made from monomode optical fibre, threshold powers may be as low as $\sim 10\mu\text{W}$ [18]. To achieve frequency shifts in the MHz region, two ring resonators would be required. If a ring were fabricated from highly birefringent fibre then each eigenmode would serve as an independent ring resonator, which could be an even more attractive solution.

5.3 Two frequency lasers.

This design utilises a laser source which has two orthogonally polarised modes at slightly different optical frequencies. Hence, the frequency 'shift' is already present at the source and separation of the two modes may be achieved using a polarisation sensitive optical fibre coupler. A commercially available visible helium neon dual mode source has been used in experiments, by other workers in the group, for a range of sensor projects [19,20], and a two-frequency infra-red source ($\lambda = 1.33\mu\text{m}$) is being developed in the group.

5.4 Two spatial mode filter.

One of the members of the optics research group has been working on polished fibre devices, and he has manufactured a polished coupler with one monomode infra-red fibre in one polished half, and a monomode helium neon fibre in the other. When the infra-red fibre is illuminated with helium-neon light it supports both of the lowest order spatial modes. The coupler can be aligned such that the light in the LP₁₁ mode couples across to the helium-neon fibre, while the LP₀₁ light is simply transmitted. This device thus forms a modal filter suitable for use at the output of a Stanford-type two-mode fibre frequency shifter, to give a monomode shifted output. The performance of the device was investigated utilising a static LP₀₁-LP₁₁ coupler, and while slightly unstable in its prototype arrangement, it could be ruggedised with little further development. The polished couplers may also provide an alternative design for a twin-core type fibre shifter. If two monomode fibres with slightly different propagation constants are polished and held in close proximity at the polished region, then a flexure wave can be excited on one fibre to cause periodic bending within the polished region and induce coupling between the cores. The interaction region is only small (few millimetres) and the device is likely to be rather delicate. A frequency shifter based on similar concept was reported at OFS 7 [21].

Acknowledgement.

We would like to acknowledge the help of the University glassblower, Mr S. Gilbert, and the Physics Laboratory administration, secretarial and technical staff.

References

- [1] Jackson D.A. and Jones J.D.C, 1987, 'Fibre optic sensors'. *Optica Acta* 33, No.12, p.1469-1503.
- [2] Risk W.P., Kino G.S., Shaw H.J and Youngquist R.C, 1984, 'Acoustic fibre-optic modulators'. Paper AO-5, IEEE Symposium on Sonics and Ultrasonics, Atlanta Ga.
- [3] Risk W.P., Kino G.S and Shaw H.J., 1986, 'Fibre optic frequency shifter using a surface acoustic wave incident at an oblique angle'. *Optics Letters*, 11, No.2, pp.115-117.
- [4] Ji J., Uttam D. and Culshaw B., 1986, 'Acousto-optic frequency shifting in ordinary single mode fibre'. *Electron.Letts.*, 22, No.21, pp.1141-1142.
- [5] Kim B.Y., Blake J.N., Engan H.E. and Shaw H.J., 1986, 'All-fibre acousto-optic frequency shifter', *Optics Letters*, vol.11, No.6, pp.389-391.
- [6] Pannell C.N., Tatam R.P., Jones J.D.C. and Jackson D.A., 1988, 'A fibre-optic frequency shifter utilizing travelling flexure waves in birefringent fibre'. *Journal of the Institution of Electronic and Radio Engineers*, Vol.58, No.5, pp.592-598.
- [7] Yijian C., 1989, 'Acousto-optic frequency shifter using coaxial fibres'. *Optical and Quantum Electronics*, 21, pp.491-498.
- [8] Greenhalgh P., Foord A. and Davies P.A., 1990 'Fibre-optic frequency shifters'. Paper 8, Proc. Fibres '90, Olympia, London, April 26, 1990.

- [9] Redwood M., 1960, "Mechanical Waveguides". Pergamon press.
- [10] Yariv A. and Yeh P., 1984 "Optical waves in crystals" .John Wiley and Sons.
- [11] Pannell C.N., 1988,"Fibre-optic laser doppler velocimetry" . Ph.D. Thesis, University of Kent at Canterbury.
- [12] Engan H.E., Kim B.Y., Blake J.N. and Shaw H.J., 1988, 'Propagation and optical interaction of guided acoustic waves in two-mode optical fibers' . JI Lightwave Technol., 6, No.3, pp.428-436.
- [13] Blake J.N., Kim B.Y.,Engan H.E., and Shaw H.J., 1987,' Analysis of intermodal coupling in atwo mode fibre with periodic microbends'.Optics Letters 12, No.4, pp.281-283.
- [14] Boyd G.D., Coldren L.A. and Thurston R.N., 1975, 'Acoustic waveguide with a cladde core geometry'. Applied Physics Letters, 26, No.2, pp.31-34.
- [15] Kim B.Y., Blake J.N., Huang S.Y. and Shaw H.J., 1987, 'Use of highly elliptical core fibers for two-mode fiber devices'. Optics Letters, 12, No.9, pp.729-731.
- [16] Boyd G.D., Coldren L.A. and Thurston R.N., 1975,'Acoustic waveguide with cladde core geometry'. Applied Physice Letters, 26, No.2, pp.31-34.
- [17] Culverhouse D.C., Farahi F., Pannell C.N. and Jackson D.A., 1989,'Potential of stimulated Brillouin scattering as sensing mechanism for distributed temperature sensors.' and 'Stimulated Brillouin scattering : A means to realise a tunable microwave generator or distributed temperature sensor'. Electronics Letters, 25, No. 14, pp. 913-916.
- [18] Kadiwar R. and Giles I.P., 1989,'Effects of stimulated Brillouin scattering on the performance of polarisation-maintaining all fibre ring resonators'. Optics Letters, 14, No.6.

- [19] Bartlett S.C., Farahi F., and Jackson D.A., 1990, 'A dual resolution non-contact vibration and displacement sensor based upon a two wavelength source'. *Rev. Sci. Instrum.*, **61**, No.3, pp.1014-1017.

- [20] Bartlett S.C., Farahi F., and Jackson D.A., 1990, 'Current sensing using Faraday rotation and a common path optical fibre heterodyne interferometer'. *Rev. Sci. Instrum.*, **61**, No.9, pp.2433-2435.

- [21] Hotate K., and Fukuchi K., 1989, 'Fiber-coupler type optical frequency shifter'. *Proc. Optical Fibre Sensors 7*, Sydney, Australia, pp.293-296.